

Radar and Optical Depth Retrieval of Marine Stratocumulus Cloud Properties Using Les Modelling

By
Matthew A. Rogers and Graeme L. Stephens

Department of Atmospheric Science
Colorado State University
Fort Collins, Colorado

Research supported by NASA research grant NAS5-99237 and DOE grant DE-FG02-ER63323.



**Department of
Atmospheric Science**

Paper No. 736

**RADAR AND OPTICAL DEPTH RETRIEVAL OF MARINE
STRATOCUMULUS CLOUD PROPERTIES USING LES MODELLING**

Matthew A. Rogers and Graeme L. Stephens

Research Supported by NASA Research Grant
NAS5-99237 and DOE Grant DE-FG02ER63323

Department of Atmospheric Science
Colorado State University
Fort Collins, Colorado 80523-1371

May 2002

Atmospheric Science Paper No. 736

ABSTRACT

RADAR AND OPTICAL DEPTH RETRIEVAL OF MARINE STRATOCUMULUS CLOUD PROPERTIES USING LES MODELLING

A computation of radar reflectivity and optical depth is performed using synthesized data from a Large-Eddy Simulation (LES) model simulating a PBL-topped, precipitating marine stratocumulus cloud layer. Radar reflectivity is computed as the sum of the cloud and drizzle components of reflectivity; the former by integrating over a gamma droplet size distribution (Clark, 1974) and the latter by integrating over a Marshall-Palmer (1948) rain droplet size distribution. The modelled results are compared with optical depth retrievals on the modelled cloud, and the relationship between radar reflectivity and cloud optical depth is examined with regard to the precipitation properties (drizzle/non-drizzle) of the cloud. Application of the data to an improved microphysical retrieval using optical depth and radar reflectivity are made for drizzling marine stratocumulus, after Austin and Stephens (2000.)

The LES model used in the study is the CSU-CIMMS LES model written by Marat Khairoutdinov. This model utilizes a standard LES dynamical framework, a variety of radiation packages, and for this study, a bulk microphysics package specially tuned for planetary boundary layer (PBL)-topped marine stratocumulus clouds. The model runs on a standard, orthogonal LES grid measuring 3.0 km in length and width, and 1.25 km in height. The model grid measures 75 m in the horizontal, and 25 m in the vertical. Model initialization is based on environmental conditions recorded during field research campaigns: specifically, using the

environmental conditions of the Nicholls (1984) study of North Atlantic marine stratocumulus, as described in Khairoutdinov (1998.)

The CloudSat Antecedent retrieval described by Austin and Stephens (2000) is used to retrieve cloud effective radius and liquid water path from the synthesized radar reflectivity and optical depth fields generated by the LES simulations. These retrieved parameters are then compared to the modelled data, and inferences about the effect of drizzle on the observable quantities of marine stratocumulus systems, specifically, radar reflectivity, visible optical depth, and liquid water path are made.

The results show that the advent of drizzle into the marine stratocumulus system leads to a predictable increase in radar reflectivity accompanied by a decrease in visible optical depth and cloud liquid water path. These effects are seen in the behavior of the retrieval as drizzle becomes manifest in the modelled data.

Matthew Alan Rogers
Department of Atmospheric Science
Colorado State University
Fort Collins, CO 80523
Summer 2002

ACKNOWLEDGEMENTS

We are grateful to Professor Dave Randall and Professor Chandrasekaran Venkatachalam for reviewing this work. Dr. Marat Khairoutdinov provided the superlative CSU-CIMMS LES model, and additionally, was absolutely accommodating and enlightening throughout this project. Dr. Richard Austin provided the CloudSat Antecedent retrieval, radar data and experience with the Monterey experiment. His contributions to this work are most gratefully acknowledged. Dr. Philip Gabriel has provided many excellent ideas as well as a great many interesting conversations. Drs. Tristan L'Ecuyer, Angela Benedetti, and Steve Miller were fine mentors and offered advice and support, as well as many coffee-cup discussions. John Haynes, Lyle Pakula, and Chris Rozoff have provided support and illumination, and their contributions are appreciated as well. Sue Lini, Jillian L'Ecuyer, and Heather Jensen are the true heros of this research project - without their sage advice, and support, I'd never have finished on time...

This research was supported by NASA Research Grant # NAS5-99237. The CSU-CIMMS LES is developed by Dr. Marat Khairoutdinov and is supported under a U.S. Department of Energy grant: DE-FG-02ER63323.

CONTENTS

1. Introduction

- 1.1 General Importance of Marine Stratocumulus Systems
- 1.2 A Brief History of Marine Stratocumulus Research
- 1.3 Production of Cloud Hydrometeor Species in Marine Stratocumulus Clouds
- 1.4 Techniques of Radar Retrieval
- 1.5 Where This Research Fits In
- 1.6 Thesis Outline and Summary of Results

2. LES Modelling of PBL-Topped Marine Stratocumulus

- 2.1 The CSU-CIMMS LES Model
 - 2.1.a Dynamics Framework*
 - 2.1.b Radiation Code*
 - 2.1.c Cloud Microphysics*
- 2.2 Numerical Methods
- 2.3 Modelled Radar Reflectivity and Optical Depth
- 2.4 The CAVEX Experiment

3. Model Analysis: Nicholls (1984) Marine Stratocumulus Studies

- 3.1 Background and Motivation
- 3.2 'Clean' model run
 - 3.2.a Modelled Results*
 - 3.2.b Radar Reflectivity Results*
 - 3.2.c Cloud Optical Depth*
- 3.3 'Dirty' model run
 - 3.3.a Modelled Results*
 - 3.3.b Radar Reflectivity Results*
 - 3.3.c Cloud Optical Depth*
- 3.4 'No Drizzle' model run
 - 3.4.a Modelled Results*
 - 3.4.b Radar Reflectivity Results*
 - 3.4.c Cloud Optical Depth*
- 3.5 Discussion and Observed Drizzle Effects on Radar Reflectivity, Optical Depth, and Liquid Water Path

4. On the Relationship Between Optical Depth and Radar Reflectivity of Marine Stratocumulus in the Presence of Drizzle

4.1 Background and Motivation

4.2 Retrieval Results Based on Simulated Data

4.2.a 'Clean' model run

4.2.b 'Dirty' model run

4.3.c 'No Drizzle' model run

4.3 A Trial Retrieval Based on the Modelled Results

4.3.a 'No Drizzle' run

4.3.b 'Dirty' run

4.3.c 'Clean' run

4.4 Error Analysis

4.5 Effects of Drizzle on the Radar Reflectivity/Optical Depth Retrieval

5. Conclusions and Future Work

5.1 Summary

5.2 Conclusions

5.3 Future Work – On the Quantification of Drizzle Properties Based On Observations

References

Appendix A: Mie versus Rayleigh Radar Reflectivities

Chapter 1

Introduction

1.1 General Importance of Marine Stratocumulus Systems

When one looks at the family of cloud systems, regions dominated by planetary boundary layer-topped marine stratocumulus seem relatively insignificant. Monsoons, tropical cyclones, and midlatitude mesoscale convective weather systems all appear to be more compelling, each with more immediate and dramatic impact when compared to other, more prosaic systems. Yet marine stratocumulus clouds have a profound, if not obvious, impact on the global climate. This impact, which is driven in part by the discrepancy in the longwave and shortwave budget of the marine stratocumulus system, has a significant effect on the global energy budget, leading to substantial modification of the global environment as a whole.

Marine stratocumulus clouds, which cover an estimated 25-30% of the global ocean at any given time (Charlson, et al. 1987 and Warren, et al. 1988) have little impact on the global longwave energy budget, as cloud-top temperatures are sufficiently similar to surface temperatures so as not to significantly affect the outgoing longwave flux. (Khairoutdinov, 1998) The liquid water composition of the marine stratocumulus cloud, however, entails a large albedo (especially when compared to the surface and, to some extent, other cloud systems.) Such a disparity in albedo between cloudy and cloud-free systems produces a significant change in the

shortwave energy budget. It is estimated that regions enclosing a marine stratocumulus cloud system experience an increase of shortwave reflectivity of roughly 30-50%. This ultimately represents a gross imbalance between long- and shortwave radiation, leading to a cloud radiative forcing of nearly 100 W/m^2 , an appreciable fraction of the total localized energy budget of the planet. Studies (Randall *et al.*, 1984, Ramanathan *et al.*, 1989) have shown that a few percent increase of marine stratocumulus cloud cover, with its attendant increase in global albedo, would be sufficient to counter the effects of global warming, while other studies (Ramanathan *et al.*, 1989) demonstrate a similar decrease in cloud cover (and therefore albedo) would nearly double said warming. Clearly, the marine stratocumulus system warrants our attention, if not for the purpose of scientific edification alone, then at least for the purpose of understanding its significant role in the global energy budget.

And yet, we are just beginning to understand the forces that drive these cloud systems. Informal research into the nature of marine stratocumulus doubtless extends far into the past. Stringent observation methodology, however, has only been applied to marine stratocumulus research since the late 1920s. While it is clear that much research has been done in this field, it is equally clear that there is much more research yet to do.

The remainder of this introductory chapter is divided into sections including a brief history of marine stratocumulus research, a description of the mechanism of the formation of precipitation in these cloud systems, an overview of radar reflectivity research and retrieval methods based on radar reflectivity, and finally, a description of

how this study integrates the above, followed by an outline of what's to come. Readers familiar with the research genre described above may wish to skip ahead to chapter two, although the background information presented serves nicely to frame the author's background in the subject matter.

1.2 A Brief History of Stratocumulus Research

As noted by Stevens (1996), the modern study of marine stratocumulus layers is a discipline spanning the breadth of the 20th century, beginning with Dean Blake's climatological analysis of Californian marine stratocumulus in the early 1900s. Stevens also notes that one of the first measurements made of marine stratocumulus clouds was of their albedo. With the advancement of atmospheric research through aviation in the 1920s and 1930s, airborne measurement of marine stratocumulus became possible; in 1928, Blake measured the temperature inversion existing at the upper boundary of the cloud-topped mixed layer. Analyses of the nature of marine stratocumulus layers progressed in the 1940s and 1950s, and culminating in a groundbreaking study involving a one-dimensional model of marine stratocumulus conducted by D.K. Lilly in 1968. The processes described by Lilly form the foundation of modern stratocumulus research, and serve as a baseline for topics in current research, including this study. Among other topics, research on cloud-top entrainment instability, stratocumulus-to-cumulus transition, and cloud radiative properties all have in their core the ideas forwarded by Lilly. This is particularly salient when considering the state of affairs of modern stratocumulus research.

With the advent of numerical modelling via computer, the questions posed by the dynamic theories of marine stratocumulus began to be more thoroughly addressed.

The non-linear nature of cumulus convection made the numerical prognostication of such systems intractable at first (indeed, the first published paper on modern chaos theory described the innate sensitivity to initial conditions that then-contemporary cumulus models were subject to, e.g. Lorenz, 1963.) while the generally stable conditions found in marine stratocumulus clouds led to workable solutions.

As previously noted, the first approach to modelling marine stratocumulus came in Lilly's one-dimensional model in 1968. The first LES models came into being in the early 1970s with the work of Deardorff (1972) and Sommeria (1976.) However, these early LES models frequently suffered at the hands of insufficient computational power; the computers of the time simply did not have the numerical capabilities to resolve the LES-sized grid over a large enough domain. The advances in computer technology in the 1980s along with further research performed by Chin-Hoeh Moeng in 1986, saw the increase in popularity of the LES model, and by Mason's (1993) review of the LES technique, the LES model had finally come into its own. Currently, several varieties of LES models exist, and perform research on a wide variety of topics, including cellular convection, cloud-top cooling and entrainment studies, stratocumulus-to-cumulus transition, as well being used to derive parametrizations for use in global climate models. The ability to accurately resolve the motions of the atmosphere in such detail is one of the greatest strengths of the LES technique, and as such, has led to a great deal of advancement in boundary-layer meteorology over the last few decades.

1.3 Production of Cloud Hydrometeor Species in Marine Stratocumulus Clouds

The initiation of precipitation processes in the marine stratocumulus system introduces several levels of complexity with respect to the cloud microphysics and thermodynamics. Sensitivity studies applied to simulations of the marine stratocumulus-topped mixed layer (e.g. Chen and Cotton, 1987) show the relationship of drizzle on cloud liquid water content, the appreciable effects this relationship has on the cloud-top longwave cooling, and thereby the general turbulent structure of the cloud system. The effect of drizzle formation also influences the amount of cloud cover represented by the marine stratocumulus system, directly altering the cloud radiative forcing of the atmosphere. As is previously mentioned, the radiative forcing of the atmosphere by cloud cover can represent nearly 100 Wm^{-2} . The fundamental differences between precipitation hydrometeors and cloud droplets lie ultimately in the formation of each type of droplet, as is discussed presently. The immediate effects of the differences between cloud and drizzle droplets lead to observable differences in physically measurable quantities, from directly measurable parameters such as cloud liquid water content and the droplet number concentration spectra, to parameters used primarily for remote sensing, such as radar reflectivity and cloud optical depth. We present in Chapter 4 results illustrating the changes of these observable parameters as a result of drizzle formation. These changes allow for an identification of the drizzle-formation process directly, and perhaps someday to the benefit of remote retrieval of cloud microphysical parameters.

The classic model of the evolution of cloud hydrometeors is traditionally broken into two regimes: the growth of cloud droplets due to vapor deposition on cloud

nuclei, and the growth of precipitation hydrometeors by the collision-coalescence process. Salby (1996) describes the initiation of cloud droplet growth as the result of heterogeneous nucleation of water on available cloud condensation nuclei (CCN) – essentially, the formation of cloud droplets on aerosol. Certain aerosol species which exhibit favorable chemical properties such as *wettability* (the ability of an aerosol’s surface to be covered by a thin layer of water) or water solubility allow for lower vapor saturation pressures above the nuclei surfaces, enhancing vapor condensation on the surface of the droplet. Aerosol nuclei that are larger than a critical value defined by the ambient supersaturation of water vapor will *activate* and begin to grow as cloud droplets by deposition of water vapor:

$$\frac{dm}{dt} = 4\pi r^2 v \frac{d\rho_v}{dr} \quad (1.1)$$

where m is the droplet mass, r is the droplet radius, v the diffusion coefficient of water vapor, and ρ_v the density of the water vapor. This process will occur for each CCN that activates. Thus we see the importance of aerosol in the growth of cloud droplets – a larger concentration of CCN above the activation threshold will result in a larger total number of cloud droplets. Similarly, the depletion of the available vapor by the deposition growth of cloud droplets will affect the subsequent rate of growth of the cloud droplets – more activated CCN will result in smaller, but more numerous cloud droplets, as described by Khairoutdinov and Kogan (2000). For a cloud system containing a similar vapor supersaturation, but fewer activated CCN, the results are fewer, larger cloud droplets. This effect becomes important when we consider the growth of precipitation hydrometeors, and as such, we present three simulations of

marine stratocumulus cloud systems with varying initial CCN concentrations. The effect of aerosol on overall cloud hydrometeor evolution is addressed in more detail in Chapters 2 and 3.

The effect of aerosol on cloud droplet growth translates directly into an effect on the growth of precipitation hydrometeors, as mentioned presently. Given the areal effects of vapor deposition on a sphere, one may reasonably assume that the growth time for a droplet growing solely through vapor deposition is quite long indeed. In fact, the computed growth time of a droplet from nucleation to sizes comparable with drizzle might be measured in days. This is too long to explain the observed formation of precipitation droplets in time scales on the order of an hour – as such, the consensus is that growth of precipitation hydrometeors does not occur through simple vapor deposition.

As cloud droplets grow, their change in mass leads to an increase in terminal velocity of the droplet that increases as a factor of the droplet radius squared. Given that the droplet growth is an inverse function of the droplet radius to the first power, we see that in a short period of time, there will exist in the cloud a great deal of diversity in droplet fall speeds, as described by Young (1993.) This variance in the droplet fall-speed spectrum, whereby larger droplets fall faster than smaller droplets, leads to a process of droplet collision and coalescence, which leads to still larger and more massive droplets. This contributes to an increase in the droplet fall-speed spectrum, leading to further droplet collisions, etc. until droplets are large enough (and therefore have sufficiently high terminal velocities) to fall from the cloud as precipitation. This *collision-coalescence* process defines the growth of precipitation

hydrometeors based on the cloud droplet concentrations from which the precipitation begins. The parametrization of this process in the microphysical code of a model will determine the overall characterization of the cloud system as simulated, and as a direct result, the observable quantities of the cloud, as mentioned above. We will explore in detail the manner by which this process is defined in the model, and as a result, the effect this process has on the produced observable quantities we seek to understand.

1.4 Techniques of Radar Retrieval

The application of radar to cloud studies in the late 1940s embodied an important advance in the study of clouds and their microphysical properties. Applied primarily to precipitating clouds as part of tropical systems and severe thunderstorms at first, the advent of smaller radars operating at higher microwave frequencies allowed increasingly more studies on non-precipitating cloud systems. Currently, a bevy of radar systems are available to the researcher of cloud microphysical structures, including airborne and spaceborne radar systems.

A key benefit of radar systems is that they make possible the sampling of a large volume of the atmosphere with little expended effort - advances in computing power combined with a precise and comprehensive understanding of the propagation of electromagnetic signals through the atmosphere allows for very in-depth analysis of back-scattered radar energy. Such analysis is useful for understanding the bulk properties of scattering hydrometeors in the sensed domain, as well as other properties such as windspeed (as measured by doppler analysis of the returned signal.) Further insight may be gleaned through the use of a polarized radar system; differences in

radar return depending on polarized aspect of the radar beam give a great deal of information on the geometric proportions of the sensed hydrometeors. Unfortunately, beyond that point, difficulties arise in further analyses, as the nature of the radar reflectivity equation (and more specifically its dominating sensitivity to droplet size) prohibits detailed analysis of droplet distribution. In shallower clouds (such as drizzling marine stratocumulus systems, perhaps) this tendency can eliminate the ability of a radar system to retrieve accurate information about cloud droplet distributions once the larger drizzle droplets begin to dominate the radar signal returns. Without any kind of *a priori* knowledge of the cloud system it is very difficult to glean any information about the cloud microphysics beyond what is essentially an empirical rain-rate measurement. Recently, Austin and Stephens (2000) suggested a method to retrieve cloud microphysical parameters using a combination of millimeter-wave radar reflectivity and visible optical depth. The method is developed primarily for non-drizzling clouds, however; the effect of drizzle on such a retrieval (which is based on the optimal inversion technique described by Rodgers (1976)) has yet to be satisfactorily determined.

1.5 Where This Research Fits In

It is towards that goal of understanding the effect of drizzle on the marine stratocumulus system, and specifically, on cloud microphysical retrievals that this research was undertaken. We propose a symbiotic approach to this research, utilizing both modelling of marine stratocumulus cloud layer microphysical and optical properties as well as the modelling of observing systems designed to measure the properties of these clouds. By utilizing a cloud-resolving model, one has precise and

omniscient knowledge of droplet size spectra and number concentration within the model domain, and can therefore produce synthetic radar reflectivity measurements. Furthermore, the effects of the formation of precipitation on these droplet spectra and number concentration may be studied, and the effects of precipitation on the measurements of radar reflectivity, visible optical depth, and cloud liquid water path can also be addressed.

The ultimate goal of this research is, therefore, to gain a greater understanding of the nature of marine stratocumulus clouds (especially in the transition between precipitating and non-precipitating) in the framework of radar retrieval methods, specifically by investigating the nature of drizzle formation and its effect on the observable quantities of the marine stratocumulus cloud layer through analysis of a retrieval performed on modelled data.

1.6 Thesis Outline and Summary of Results

What is presented here is a brief outline of what is to come. Chapter 2 will delve into the specifics of the LES modelling technique along with the details of the CSU-CIMMS LES model used in this study, including an analysis of the model cloud and precipitation procedures. We also discuss in this chapter methods of computing radar reflectivity from modelled results based on the data provided by the model itself. Chapter 3 will present a summary analysis of the three model simulations performed in this study, and will discuss the observed effects of drizzle formation on observable parameters. Chapter 4 will detail the cloud retrieval used for this research, and present retrieval results computed using the simulated data introduced in Chapter 3, with a discussion regarding the ability to identify regions of cloud containing drizzle.

Finally, Chapter 5 presents a summary of the study's results, and forward-looking statements regarding what may be pursued using the results of this study.

To this end, we will show that simulated radar reflectivities and optical depth computed using LES models obey theoretical relationships between the two quantities, and that the relationship obtained through these simulations match well with observed relationships. We will also show that simulated cloud and drizzle reflectivities match with observed cloud and drizzle reflectivities. We perform a cloud microphysical retrieval using these simulated parameters, and show that retrieved values of LWC and effective radius match well with the modelled parameters, even in light drizzle. We will demonstrate the failure of the retrieval in heavy drizzle, and explore the manner of this failure with respect to the assumptions made in the retrieval process. Finally, we will show that optical depth and radar reflectivity may be used to discriminate between drizzling and non-drizzling marine stratocumulus systems, and furthermore, the addition of an independently-retrieved cloud liquid water path further adds to the value of this discriminating ability.

Chapter 2

LES Modelling of PBL-topped Marine Stratocumulus

We begin our study by describing in detail the model we will be using to simulate marine stratocumulus systems, presenting an overview of the observed data to which we compare the modelled results, and by defining the manner in which we compute the necessary retrieval parameters to be used in our cloud microphysics retrieval. Furthermore, we present in this chapter a theoretical analysis of the radar reflectivity/optical depth relationship and compare this analysis to observed and modelled data. We postpone detailed discussion of the retrieval itself until Chapter 4 for the sake of clarity. Practical application of the material found in this chapter is presented in Chapter 3, where we present model simulation results.

Many methods exist whereby one may study marine stratocumulus cloud systems, and although a limited number of excellent observational studies of marine stratocumulus exist (e.g. Nicholls 1984, Ackerman et al. 1995) detailed observations are lacking for the most part. Thus, we resort to detailed simulations of marine stratocumulus cloud systems using a cloud-resolving model. Utilizing such a model has many benefits, among them being the ability to reproduce many different cloud system cases realistically, and the ability to re-run a case to investigate the sensitivity of the cloud system to various changes in the environmental conditions. Since these models often involve a few key parameterizations, it is necessary to validate the particular model against observational studies for the sake of accuracy. A well-chosen and robust model will be able to reproduce the essential features gleaned from any observational study, within the limits imposed by numerical theory and

processing power.

2.1 The CSU-CIMMS LES Model

For this research, we have chosen to use the CSU-CIMMS LES model. The CSU-CIMMS LES model is a cloud resolving model described in detail in Khairoutdinov (1998.) The model has been used in several investigations of marine stratocumulus clouds, including a veracious reproduction of the Nicholls (1984) study of North Atlantic marine stratocumulus clouds, among others. Specific details of several of these experiments, including flux profiles and vertical cross sections of model output are included in the introduction sections of the following chapters - what is presented here is an overview of the model itself.

The CSU-CIMMS model is based on previous versions of the CIMMS LES model, developed at the University of Oklahoma. Previous versions of the CIMMS model utilized spectral code to compute the dynamical variables, which rendered the model unable to accurately compute advection of scalar properties without intermediate code that provided a positive-definite finite-difference scheme (based on the work of Smolarkiewicz.) Unfortunately, unless this model was run on a very small grid, the velocity grid in the finite-difference scheme became divergent, leading to commanding errors in the advection of microphysical variables through the model (Khairoutdinov, 1998.) The dynamics package of the model was re-written to address these issues, and to provide stable finite-difference representation of the entire model variable population. This package serves as the core of the model used in the current research. Additional updates to this package include modifications and advancements in the bulk-microphysics code, as well as improvements in the radiation code. The

fundamental details of the model are now briefly reviewed.

2.1.a. Dynamical Framework

The dynamic code of the CSU-CIMMS LES model is designed to average over each grid cell, with perturbation terms being parametrized as sub-grid scale (SGS) eddies. On a suitable grid spacing, these SGS terms are within the inertial subrange, and primarily serve to dissipate turbulent kinetic energy (TKE.) The description below is paraphrased from Khairoutdinov, (1998) in which the author describes the model in great detail.

The velocity fields are governed by the Navier-Stokes and continuity equations, with the assumption of an incompressible fluid in the Boussinesq approximation, as shown below:

$$\frac{\partial \bar{u}_i}{\partial t} = -\frac{\partial}{\partial x_j} (\overline{u_i u_j} + \delta_{ij} \theta_0 \bar{\pi}' + \tau_{ij}) + \delta_{i3} g \frac{\bar{\theta}_v'}{\theta_0} + \varepsilon_{ij3} f (\bar{u}_j - u_{gj}) \quad (2.1)$$

$$\frac{\partial \bar{u}_i}{\partial x_i} = 0 \quad (2.2)$$

In equation (1), u_i is the resolved wind (in standard vector notation), π is the Exner function, τ_{ij} represents the Reynolds SGS stresses, θ_v is the virtual potential temperature, θ_0 is the reference potential temperature, f is the Coriolis parameter, and u_{gj} is the geostrophic wind. For the notation used here, bars represent resolved-scale mean components while primes represent SGS perturbation components.

The CSU-CIMMS LES model represents thermodynamic processes based on liquid water potential temperature and total water content. For moist adiabatic processes, these variables are conserved, and therefore serve as ideal variables for

prognostication. θ_l is defined using the virtual liquid water static energy divided by the liquid water potential temperature, and as such, is also conserved. Thus we have the two conservation equations for thermodynamics:

$$\frac{\partial \overline{\theta_l}}{\partial t} = -\frac{\partial}{\partial x_i} (\overline{\theta_l u_i} + \tau_{i\theta}) - \frac{1}{\rho c_p} \frac{\partial F}{\partial z} + \frac{L}{c_p} \frac{\partial P}{\partial z} - w_s \frac{\partial \theta_l}{\partial z} \quad (2.3)$$

$$\frac{\partial \overline{q_T}}{\partial t} = -\frac{\partial}{\partial x_i} (\overline{q_T u_i} + \tau_{iq}) - \frac{\partial P}{\partial z} - w_s \frac{\partial \overline{q_T}}{\partial z} \quad (2.4)$$

where θ_l represents the liquid water potential temperature, q_T is the total water content, P is the total precipitation flux, F is the net radiation flux, the τ terms represent the SGS fluxes of θ_l and q_T , and w_s represents the model-scale subsidence rate.

2.1.b. Radiation Code

Currently, the model uses code developed by Chris Bretherton based on the longwave code of Herman and Goody (1976) and the shortwave code of Gierasch and Goody (1970), tuned for the Nicholls (1984) study. The model used here is a somewhat older version of the current CSU-CIMMS LES, tuned specifically for use with marine stratocumulus, and therefore does not have the benefit of readily-interchangeable radiation packages. Current versions of the CSU-CIMMS LES run either this radiation code, described below, or the newly-developed and more sophisticated CSU-BUGSRAD radiation code. For the purposes of continuity with previous research, as well as coding simplicity, this research uses the older, still valid radiation code, which we will now investigate.

The longwave code is a one-band approximation with non-exponential absorption

in water vapor and exponential absorption in liquid water. The longwave flux equation described by Bretherton in the code comes from equation 18 in Herman and Goody:

$$\begin{aligned}
F_T = & - \int_0^z \pi B(z') d\varepsilon_M [3^{1/2} m(z, z'); 3^{1/2} u(z, z')] \\
& + \pi B^* \{1 - \varepsilon_M [3^{1/2} m(z, 0); 3^{1/2} u(z, 0)]\} \\
& - \int_z^\infty \pi B(z') d\varepsilon_M [3^{1/2} m(z, z'); 3^{1/2} u(z, z')]
\end{aligned} \tag{2.5}$$

Shortwave radiation is treated as a three-band approximation with the cloud absorption coefficient calculated from the mean droplet radius computed in the model itself. The simple form of the shortwave flux in the code by Bretherton is described by equation 16 in Gierasch and Goody:

$$F_S = F_S(0)e^{-\beta\tau_s} \tag{2.6}$$

with coefficients described by Herman and Goody, and amended by Khairoutdinov.

2.1.c. Cloud Microphysics

The bulk microphysics code used for this research is a product of research performed by Khairoutdinov and Kogan (2000) on marine stratocumulus clouds systems, and as such, is highly optimized to study warm cloud-topped mixed layer clouds. The microphysics package is based on the methodology of Kessler (1969) and is therefore partitioned into cloud and precipitation components. The prognostic microphysical equations are based on several considerations: that the drizzle initiation process is sensitive to the characteristic size of the droplet population, that for a given liquid water content (LWC), the characteristic droplet size is determined by the droplet concentration (which in turn is determined by ambient CCN count), and that

the droplet integral radius (the product of the droplet mean effective radius and the mean droplet concentration) is useful for computation of the droplet spectral dispersion. These three parameters, namely, characteristic droplet size, droplet concentration, and droplet integral radius, form the foundation of the microphysical scheme used in the model, and follow the research of Clark (1974.) The complete set of parameters used in the microphysics package include CCN count n , cloud water mixing ratio q_c , cloud drop concentration N_c , integral radius of cloud droplets R_c , drizzle water mixing ratio q_r , and drizzle droplet concentration N_r . The fundamental conservation equations governing the microphysical processes are:

$$\frac{\partial n}{\partial t} = -\frac{\partial u_i n}{\partial x} - \left(\frac{\partial N_c}{\partial t}\right)_{activ} + \left(\frac{\partial N_c}{\partial t}\right)_{evap} + \frac{\partial}{\partial x_i} K \frac{\partial n}{\partial x_i}, \quad (2.7)$$

$$\frac{\partial q_c}{\partial t} = -\frac{\partial u_i q_c}{\partial x_i} + \left(\frac{\partial q_c}{\partial t}\right)_{activ} + \left(\frac{\partial q_c}{\partial t}\right)_{cond} - \left(\frac{\partial q_r}{\partial t}\right)_{auto} - \left(\frac{\partial q_r}{\partial t}\right)_{accr} + \frac{\partial}{\partial x_i} K \frac{\partial q_c}{\partial x_i}, \quad (2.8)$$

$$\frac{\partial N_c}{\partial t} = -\frac{\partial u_i N_c}{\partial x_i} + \left(\frac{\partial N_c}{\partial t}\right)_{activ} - \left(\frac{\partial N_c}{\partial t}\right)_{evap} - \left(\frac{\partial N_c}{\partial t}\right)_{accr} - \left(\frac{\partial N_c}{\partial t}\right)_{auto} + \frac{\partial}{\partial x_i} K \frac{\partial N_c}{\partial x_i} \quad (2.9)$$

$$\frac{\partial R_c}{\partial t} = -\frac{\partial u_i R_c}{\partial x_i} + \left(\frac{\partial R_c}{\partial t}\right)_{activ} + \left(\frac{\partial R_c}{\partial t}\right)_{cond} + \frac{\partial}{\partial x_i} K \frac{\partial R_c}{\partial x_i}, \quad (2.10)$$

$$\frac{\partial q_r}{\partial t} = -\frac{\partial u_i q_r}{\partial x_i} + \frac{\partial V_{q_p} q_r}{\partial z} + \left(\frac{\partial q_r}{\partial t}\right)_{cond} + \left(\frac{\partial q_r}{\partial t}\right)_{auto} + \left(\frac{\partial q_r}{\partial t}\right)_{accr} + \frac{\partial}{\partial x_i} K \frac{\partial q_r}{\partial x_i}, \quad (2.11)$$

$$\frac{\partial N_r}{\partial t} = -\frac{\partial u_i N_r}{\partial x_i} - \left(\frac{\partial N_r}{\partial t}\right)_{evap} + \left(\frac{\partial N_r}{\partial t}\right)_{auto} + \frac{\partial}{\partial x_i} K \frac{\partial N_r}{\partial x_i}. \quad (2.12)$$

Again, u_i represents the resolved wind velocity components, K is the eddy diffusivity coefficient (from the dynamics code), and V represents fall velocities computed using both N and q . Subscripts in parametrized differentials are as follows:

activ denotes droplet activation (a source of cloud droplet growth due to nucleation of CCN,) *evap* denotes droplet evaporation, *cond* denotes droplet condensation from the vapor phase, *auto* denotes the ‘autoconversion’ of cloud water to precipitation, and *accr* denotes accretion of cloud droplets to form precipitation. These parameterized differentials, namely $()_{activ}$, $()_{evap}$, $()_{cond}$, $()_{auto}$, and $()_{accr}$ are described in detail in Khairoutdinov and Kogan (2000) and were numerically computed using an LES model based on the same dynamical framework, but utilizing a bin-microphysics package.

As stated above, the CSU-CIMMS LES model uses a bulk microphysics package based on the scheme of Kessler (1969.) One of the unique features of the CSU-CIMMS LES is the statistically-based initial generation of rain and drizzle (termed *autoconversion*) based on the cloud water content. Although computationally more expensive, explicit microphysics schemes do not suffer from the need to “initiate” precipitation, which is of course, an artifact of partitioning the cloud water in the manner of Kessler. However, sophisticated statistical analysis of the output of many, many explicit-microphysics LES simulations, when applied to the autoconversion parametrization in the Kessler scheme, allows for a more seamless transition from cloud water to drizzle in the bulk microphysical package. Thus one obtains the the computational efficiency of bulk microphysics combined with the realistic droplet spectra as found in explicit schemes.

The trade-off is that the resulting bulk scheme is highly tuned to a specific type of cloud, however, for studies representing cloud systems that fall within the regime described by the statistical analysis, the results obtained will be very useful.

Khairoutdinov and Kogan (2000) compare model simulations of marine stratocumulus, both drizzling and non-drizzling, using the computed bulk microphysics parametrizations with explicit model simulations, and find the agreement between the two models to be quite good indeed.

Formation of drizzle in the CSU-CIMMS LES model is governed by two processes: autoconversion of cloud droplets, and accretion of smaller droplets to larger drizzle droplets. The parametrization of the autoconversion process is described in detail in Khairoutdinov and Kogan (2000) and is based on statistical regression of over 100 000 drop spectra computed by explicit-microphysics LES simulations. The autoconversion process is governed by the initialization file in the model – the user may specify the time-step at which the autoconversion code engages. One may trivially turn the autoconversion process off by setting this time step to coincide with the last time step in the model. Accretion of drizzle, defined as the collision of droplets larger than 25 μm with droplets smaller than 25 μm is similarly parametrized in the model by a statistical regression of explicit-microphysics LES simulations. Other parameters governing drizzle as seen in equations 2.11 and 2.12 include droplet condensation, which can affect the drizzle water content, and droplet evaporation, which effects the drizzle droplet number concentration.

2.2 Numerical Methods

As described in Khairoutdinov (1998), the CSU-CIMMS LES uses an Arakawa C-grid advection scheme in flux form with periodic boundary conditions in the horizontal dimension, a “sponge-layer” upper boundary, and a “slippery” bottom surface with a definable friction coefficient. Closure order in the advection scheme is

definable from second to fifth order. Time integration in the model follows a third-order Adams-Bashforth scheme. Subgrid-scale (SGS) diffusion is determined by second-order centered differences, while pressure perturbations are computed by a fast-Fourier transform (FFT) solution of Poisson's equation.

The model domain parameters will be described in detail shortly. The model domain is 3x3x1.25 km, with grid spacing of 75 meters in the horizontal and 25 meters in the vertical, or a grid of 40x40x50 gridpoints per model volume. The model runs on a dynamic time step of 3 seconds, with a microphysical time step of 0.1 seconds. The simulations last for three hours of model-time, with output statistics writing every one minute of simulated time. Thus, the total number of gridpoints that exist for one complete model run is 40x40x50x180, or 14 400 000 gridpoints per variable. The model runs on a PC workstation with an 80x86-based processor clocked at 950 MHz, with 768 MB of system RAM. A complete simulation requires roughly 600 MB of disk to capture the relevant statistics, and requires ~9 hours of computation time.

2.3 Modelled Radar Reflectivity and Optical Depth

One of the key benefits of using a model is the ability to simulate physical measurements, such as radar reflectivity, from the model output. Where a modeller of the atmosphere has complete and final knowledge of every detail inside the model, the observer of the real atmosphere must frequently rely on data *inferred* from measurements of physical parameters that merely relate to the relevant system being studied. In order to make comparisons between modelled data and measurements, therefore, it is necessary to compute from the modelled data a parameter that an

observer might actually measure. In this case, we use the computed microphysical parameters of the model to determine the radar reflectivity.

One must carefully consider, however, the manner in which the simulated data are created - any error or miscalculation imparts significant bias in the results, which usually invalidates any comparison made with real data. In the case of creating synthetic radar reflectivity data, for instance, one must carefully consider the geometric properties of the remotely sensed targets with respect to the wavelength of the radar being used to remotely sense with. The canonical equation by which radar reflectivity is calculated via drop size distribution and droplet diameter is usually written as:

$$Z = \int N(D)D^6 dD \quad (2.13)$$

where $N(D)$ is the drop size distribution, and D is the droplet size over which the integral is performed. One sees directly the dominating dependence of radar reflectivity on droplet diameter D , which is a direct consequence of the assumption of Rayleigh scattering.

We make the Rayleigh assumption for the simplicity of calculation of our radar reflectivity; in order to do this, we must justify our assumption. The Rayleigh approximation is valid for systems when the size parameter

$$\chi \equiv \frac{2\pi r}{\lambda} \ll 1. \quad (2.14)$$

where r is the droplet radius, and λ is the wavelength. For 94 GHz systems ($\lambda \sim 3$ mm), the Rayleigh approximation is valid for droplets less than ~ 20 - 47 μm , depending on what one defines as much less than unity. As such, the drizzle

produced by the model simulations begin to strain the limits of the Rayleigh approximation – the maximum drizzle droplet radius recorded was a 50.5 μm droplet produced in the ‘clean’ simulation. The mean drizzle droplet radius for the ‘dirty’ case was 38 μm , while the mean for the ‘clean’ case was 45 μm . Analysis of the behavior of the Rayleigh approximation as the size parameter begins to depart from the bounds defined by equation 2.14, however, show that the initial impact of slightly violating the Rayleigh assumption is small (L’Ecuyer and Benedetti, personal communication.) This is demonstrated in Appendix A. Computations of the ratio of radar reflectivity factor η computed using the full Mie theory show that for drizzle droplet effective radii representative of the rainrates simulated in the ‘clean’ simulation, the Rayleigh approximation of radar reflectivity factor overestimates the actual Mie radar reflectivity factor by only 8%. This value of 8%, which corresponds to drizzle effective radii of nearly 180 μm , represents a ‘worst-case’ scenario – on the average, the bias is presumed to be even smaller than 8%, and as such, we feel confident that the Rayleigh approximation is valid for the computations performed.

The CIMMS-LES model delineates between cloud droplets and precipitation droplets by breaking them into separate categories with code that governs the transition from droplet to drizzle as described by Khairoutdinov and Kogan (2000.) Cloud droplets follow a modified gamma distribution as described by Clark (1974.) The model defines the distribution as:

$$f(r) = \frac{N_c \beta^{\gamma+1}}{\Gamma(\gamma+1)} r^\gamma \exp[-\beta r] \quad (2.15)$$

with N_c as the cloud droplet number concentration (predicted from equation 2.9), r as

the droplet radius, and γ defined in the microphysics scheme by the following:

$$\gamma = \frac{5 - 2P + \sqrt{(8P + 1)}}{2P - 2}, \quad (2.16)$$

$$P \equiv \frac{3\rho_a q_c N_c^2}{4\pi\rho_w R_c^3}$$

where ρ_w is the density of water, ρ_a is the density of air, q_c is the cloud liquid water mixing ratio prognosed from equation 2.8, and R_c is the droplet integral radius that follows from equation 2.10. Combining this with the reflectivity equation yields a complete equation of:

$$Z = \frac{N_c \beta^{\gamma+1}}{2^\gamma [\Gamma(\gamma+1)]} \int_0^\infty D^{\gamma+6} \exp\left[-\frac{\beta}{2} D\right] dD \quad (2.17)$$

This integral is easily solved by the application of gamma functions, yielding a cloud-component radar reflectivity of

$$Z_{cloud} = 128 \frac{N_c}{\beta^6} \prod_{n=1}^6 (\gamma + n) \quad (2.18)$$

We compute the radar reflectivity of drizzle according to the Marshall-Palmer (1948) distribution for raindrops:

$$N(D) = N_0 e^{-\Lambda D} \quad (2.19)$$

Combining this with the radar reflectivity equation yields:

$$Z = N_0 \int_0^\infty e^{-\Lambda D} D^6 dD \quad (2.20)$$

which is solved analytically. The solution yields a drizzle reflectivity component of:

$$Z_{drizzle} = 720 \frac{N_0}{\Lambda^7} \quad (2.21)$$

where Λ may be found analytically through a power law using the computed surface rain rate as described in Marshall and Palmer (1948.) It is interesting to note that while drizzle liquid water contents represent only a fraction of the total liquid water content of the model, it represents the **bulk** of the radar reflectivity computed for the clean modelled case, as is shown in Chapter 3.

Given that the Marshall-Palmer distribution is primarily used for warm-rain processes, the question arises of whether the Marshall-Palmer distribution is valid for drizzling marine stratocumulus systems. Khairoutdinov and Kogan (2000) examined the ratio of precipitation fallspeed computed from droplet number concentration as well as from droplet water content, and found this ratio to be smaller than the theoretical value obtained using the Marshall-Palmer distribution, and as such, concluded that the Marshall-Palmer distribution was not valid for the kind of droplet fallspeeds computed in their study. Chen and Cotton (1987) however, used an exponential dropsize distribution for their study of marine stratocumulus, and obtained reasonable results. Clearly, the question of what dropsize distribution to use when computing radar reflectivity is paramount, as the distribution used will determine the solution of the radar reflectivity equation. For this study, the intent was to compare modelled results with a retrieval performed on observational data - specifically, observations made during the CAVEX campaign, which we present in the next section. The computed radar reflectivity should ideally behave in a manner similar to real-world observations. In order to investigate the effects of dropsize

distribution choice on the computed radar reflectivity, a trial computation using the simulated data from the ‘clean’ simulation described in Chapter 3 was performed, utilizing both the Marshall-Palmer dropsize distribution and a log-normal distribution used for computation of radar reflectivity described by Fritsch, *et al.* (1995). Figure 2.1 shows a comparison of computed radar reflectivity probability density functions and the CAVEX data obtained on 24 June, 1999. It is important to note that the total number of measurements are not necessarily representative between the CAVEX data and the simulation; specifically, the simulated cloud exhibited more drizzle pixels than did the CAVEX case. What is illuminating, however, are the general features found between the diagrams. Both the CAVEX data and the computed reflectivities show cloud reflectivity maxima approximately between -20 and -30 dBZ, with drizzle signatures broadly in the range of -10 to $+10$ dBZ. Given the relative similarity of the radar reflectivity maxima produced by the Marshall-Palmer and the log-normal distribution, we see that for this simulation, the choice of drizzle dropsize distribution is not as crucial as was originally thought. As such, we choose the numerically simpler Marshall-Palmer distribution for our calculations.

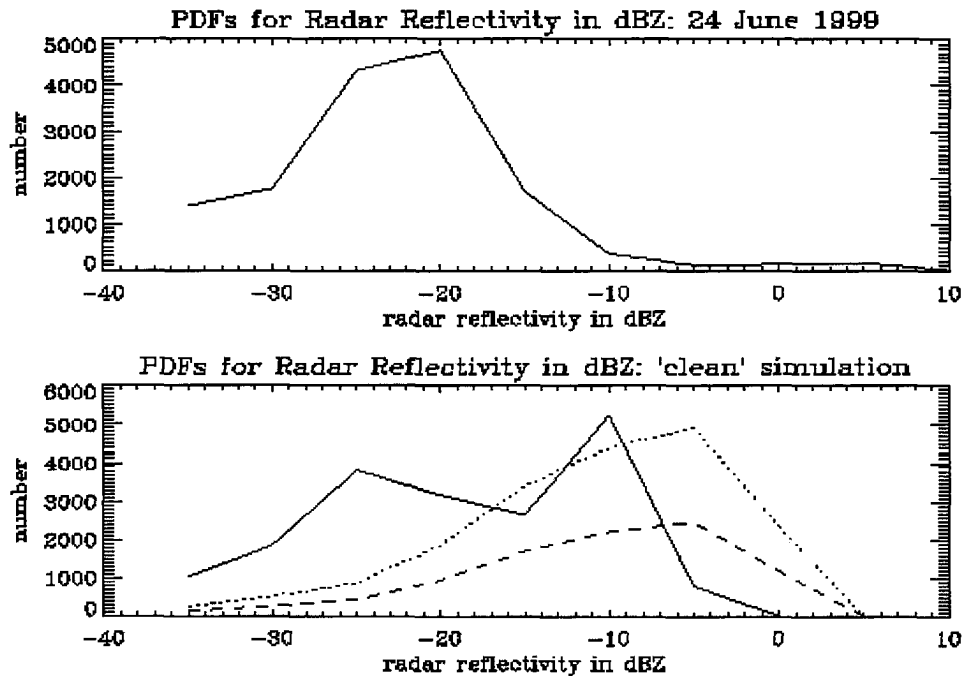


Figure 2.1 Probability-density functions of radar reflectivity. Top figure is total radar reflectivity observed from the CAVEX drizzle case of 24 June 1999. Bottom figure represents computed radar reflectivities using a Marshall-Palmer distribution (dashed line), the log-normal distribution of Fritsch, et al (1995) (dotted line.) The solid line represents the reflectivity of cloud droplets

Results similar to those shown in Figure 2.1 were obtained from a trial computation of radar reflectivity for the ‘dirty’ simulation; the plot for this trial is omitted for the sake of brevity.

Once computed, the radar reflectivity for the cloud water and drizzle are summed to compute the total reflectivity. As is seen in Figure 2.1, there appears to be a roughly bi-modal distribution of radar reflectivities, with cloud droplet maxima around -25 dBZ and drizzle/pre-drizzle reflectivity maxima around -10 dBZ. These reflectivity maxima agree with empirical studies (Baedi, Boers, and Russchenberg, 2001) of African marine stratocumulus cloud systems involving airborne measurement of droplet distributions (utilizing FSSP and 2D-Gray probes).

For the purpose of comparison to visible optical depth, the integrated radar reflectivity is computed by spatially averaged over the modelled domain before

vertically integrating over reflectivity. This provides a spatial 'footprint' of radar reflectivity similar to what an airborne/spaceborne radar instrument would 'see' and allows for direct comparison to actual airborne measurements of radar reflectivity.

Optical depth is commonly introduced (e.g. Stephens, 1993) as the vertically-integrated volume absorption coefficient of the atmosphere at a given frequency. The canonical definition of optical depth is thus:

$$\tau(z_1, z_2) = \int_{z_1}^{z_2} k_{\nu, \nu} dz \quad (2.22)$$

where $k_{\nu, \nu}$ is the volume absorption coefficient at frequency ν . For macroscopic interaction of radiation with matter, we define the *extinction* to be the sum of absorption and scattering of matter, and define optical depth as the vertically integrated volume coefficient of extinction:

$$\tau = \int_{\Delta z} \sigma_{ext} dz \quad (2.23)$$

where

$$\sigma_{ext} = \int_0^{\infty} \pi r^2 n(r) Q_{ext} dr \quad (2.24)$$

For values of ν representative of the visible spectrum, we can assume the large particle limit for Q_{ext} for cloud droplets, and, by combining equations (2.23) and (2.24), define the cloud optical depth as:

$$\tau \approx 2 \int_{\Delta z} \int_0^{\infty} n(r) \pi r^2 dr dz \quad (2.25)$$

Thus we see the similarity of the cloud optical depth and radar reflectivity: both are integrated moments of the droplet size distribution. We explore the theoretical nature of this relationship in the next section.

The CSU-CIMMS LES model computes directly the visible optical depth for use in the radiation code; as such, no additional calculations of optical depth are necessary for the analysis presented in this research.

2.4 The CAVEX experiment

Having computed radar reflectivity and cloud visible optical depth from modelled parameters, we then apply the computed values to an optimal-estimation cloud microphysical retrieval. Tentatively titled the CloudSat Antecedent Retrieval and written specifically to use 94-GHz radar data and visible optical depth measurements as input parameters, the retrieval returns cloud microphysical properties using an optimal estimation scheme similar to one described by Rodgers (1976.) The retrieval, as its name implies, is designed for use with CloudSat remotely retrieved data and is compatible with other observational systems that use the same parameters. A preliminary validation of the retrieval scheme was performed in late 1999; a description of this validation experiment is presented here.

As described in Austin *et al.* (2001) the CloudSat Antecedent Validation Experiment (CAVEX) was conducted off the coast of Monterey, California, during the months of June and July, 1999. The study was part of a larger experiment initiated by Dr. Bruce Albrecht of the University of Miami, and as such, was able to take advantage of airborne research flights of the stratus decks already being performed, while adding an additional aircraft for remote sensing of the cloud layer

from above. Instruments used to simulate CloudSat measurements include the JPL/UMass Airborne Cloud Radar (ACR), as described by Sadowy *et al.* (1997), and the Colorado State University Scanning Spectral Polarimeter (SSP) described by Stephens *et al.* (2000.) The SSP instrument was used to calculate visible optical depths using measured values from the 0.583 and 0.609 μm , as described by Miller *et al.* (2000.)

Flying below the remote sensing instrumentation aircraft, in a ‘stacked’ formation, was the MCSE Twin Otter aircraft, which was outfitted with the Particle Measuring Systems Forward Scattering Spectrometer Probe (FSSP) and a Gerber Scientific Particle Volume Monitor (PVM) probe, among other instruments. The FSSP probe measures cloud/drizzle droplet size, while the PVM probe measures cloud water content. Radar data from the above-cloud aircraft is matched with sensed data from the in-cloud aircraft using GPS data.

What follows is a brief synopsis of representative experiments flown during CAVEX, describing radar reflectivity and optical depth measurements made during the field campaign. We present a theoretical analysis of the relationship between integrated radar reflectivity and optical depth, based on the gamma dropsizes distribution, and compare this relationship to CAVEX data *and* results computed from model simulations, presented in Chapter 3. We show good agreement between the results of the simulations, observed CAVEX data, and the theoretical relationship to be developed shortly.

The equation for visible optical depth computed for cloud droplets is:

$$\tau \cong \int_{z_b}^{z_t} \int_0^{\infty} 2\pi n(r)r^2 dr dz \quad (2.26)$$

where $n(r)$ represents the cloud droplet size distribution, r is the cloud radius, and z_b and z_t represent cloud bottom and cloud top heights, respectively. Using the gamma droplet size distribution (equation 2.15) we compute the cloud optical depth to be:

$$\tau = \int_{z_b}^{z_t} \frac{2\pi N_c}{\beta^2} \prod_{n=1}^2 (\gamma + n) dz \quad (2.27)$$

Similarly, we can compute integrated radar reflectivity by integrating equation (2.18) over the cloud depth described in equation (2.22):

$$IZ = 10 \log_{10} \left[\int_{z_b}^{z_t} 128 \frac{N_c}{\beta^6} \prod_{n=1}^6 (\gamma + n) dz \right] \text{ in dBZ} \quad (2.28)$$

We can plot the theoretical relationship between equations (2.24) and (2.23) by assuming representative values for the droplet dispersion constant γ and droplet number concentration N_c taken from the simulations presented in Chapter 3. Here, we assume $\gamma=3$ and $N_c = 87 \text{ cm}^{-3}$ based on the non-drizzling and lightly drizzling simulation data. We then vary the inverse radius parameter β over a range of values which are representative of optical depths measured in the CAVEX experiment and simulated in the model runs, and compare the computed integrated radar reflectivity values to the optical depths thus derived. Figure 2.2 presents this theoretical relationship.

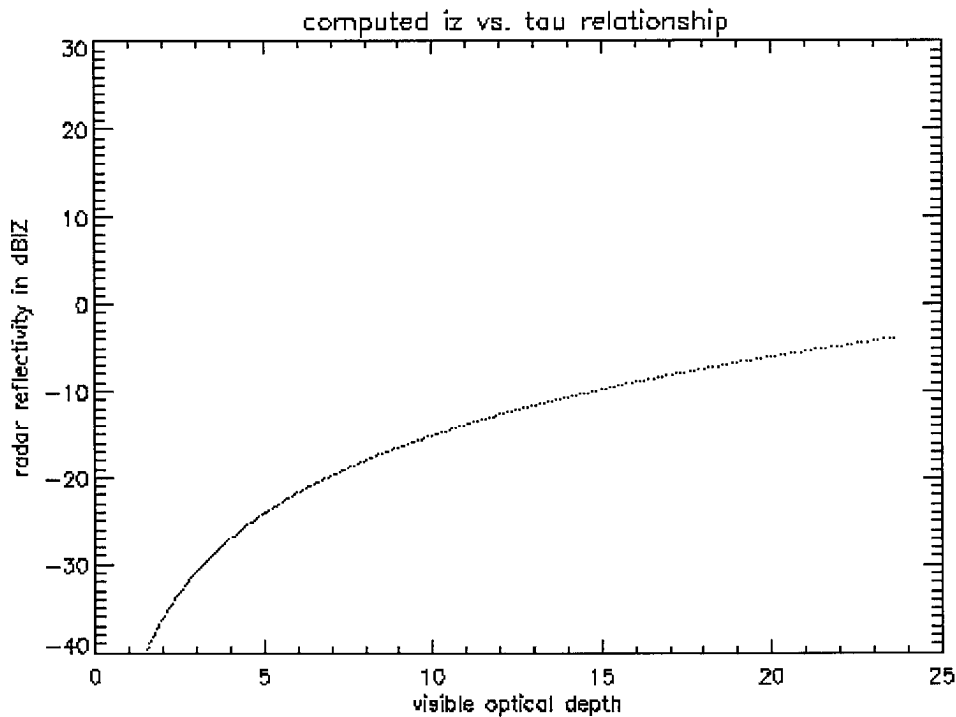


Figure 2.2 Computed integrated radar reflectivity-optical depth relationship using the gamma drops size distribution.

Generally, we observe that at larger optical depths, the integrated radar reflectivity asymptotically approaches ~ -5 dBZ. Realistically, this value would be somewhat lower, as characteristic radii consistent with these high optical depths violate the Rayleigh assumption of the radar reflectivity equation – the equivalent radar reflectivities computed from Mie theory are lower than those computed through the Rayleigh assumption. The smallest optical depths (below ~ 6) show the greatest decrease in integrated radar reflectivity. The asymptotic behavior of cloud reflectivity as a function of optical depth supports the partitioning suggested by Baedi, Boers and Russchenberg (2001), as the maximum values of cloud reflectivity indeed do not realistically exceed -10 dBZ. We now compare modelled and observational data to this theoretically-derived relationship.

Two cases from the CAVEX experiment are considered: the first, a non-drizzling case from the 19th of June, and the second, a drizzle-containing case from the 24th of June. Radar data from the CAVEX experiment was provided to the author by Richard Austin, who received the data from Stephen Sekelsky. Optical depth information was provided by Richard Austin. Processing of the data was limited to removal of the ground reflection signature, and time-matching of the radar data to corresponding optical depth data. Figure 2.3 shows the comparison of the three model runs and the Monterey data.

Generally, the comparison of the two data sets show the same fundamental relationship between cloud optical depth and integrated radar reflectivity as the theoretical calculation. The ‘clean’ simulation, presented in section 3.2, produced heavy drizzle, and as such, is expected to exhibit different behavior than a non-drizzling simulation; however, the ‘dirty’ and ‘no-drizzle’ simulations, presented in sections 3.3 and 3.4, respectively, behave in the manner expected from theoretical analysis of the relationship between optical depth and radar reflectivity – asymptotic behavior at high optical depths combined with decreases in radar reflectivity at lower optical depths. The modelled clouds are generally thicker than the observed Californian stratocumulus, as were the North Atlantic stratocumulus the model was simulating – we see this difference in the optical depth measurements of the observed and the modelled clouds. It would be interesting to perform a simulation of thinner stratocumulus such as those observed during the CAVEX campaign to observe the relationship between optical depth and integrated radar reflectivity. We would expect such a simulation to reproduce the observed results presented above.

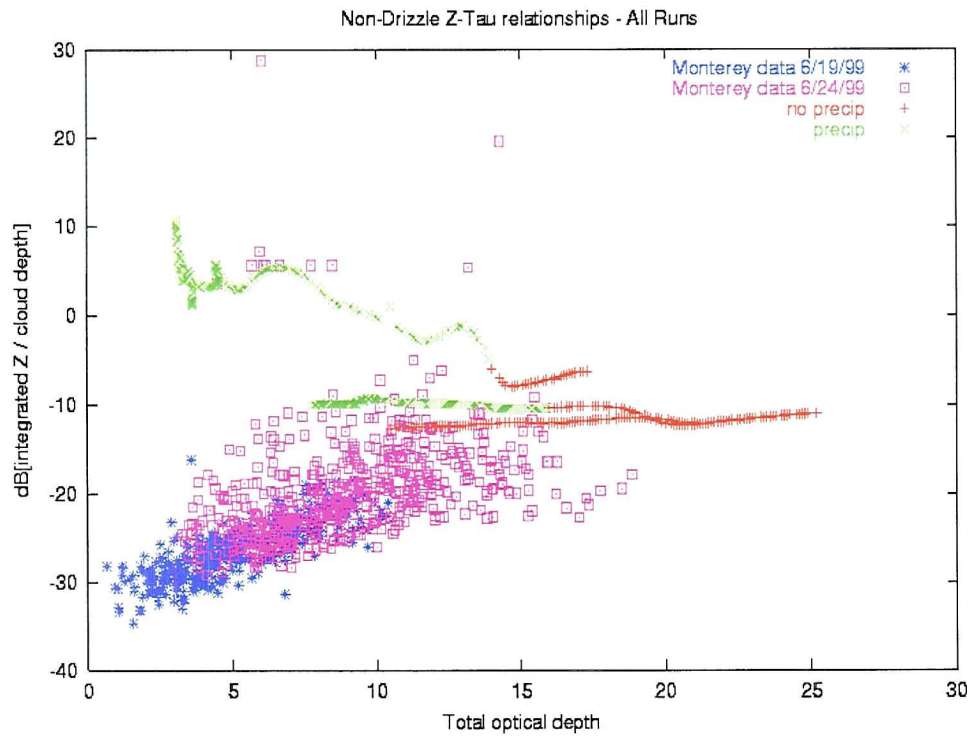


Figure 2.3. Montage of radar reflectivity/optical depth for the three model runs superimposed on CAVEX radar/optical depth data from Richard Austin. Green and red symbols denote the CSU-CIMMS LES model data, while blue and magenta symbols represent CAVEX data. CAVEX data courtesy of Richard Austin and Stephen Sekelsky.

Chapter 3

Model Analysis: Nicholls (1984) Marine Stratocumulus Studies

Having derived the necessary quantities to be used in our analysis, we perform simulations of marine stratocumulus based on the observational study of Nicholls (1984). We also compute from the modelled results the radar reflectivity for cloud and drizzle water, and compare these computations to field observations. We show a favorable comparison between our results and observed quantities. The simulations presented in this chapter are used in the retrievals described in Chapter 4. The simulations presented in this chapter were designed to explore the effects of aerosol on cloud and drizzle formation. This is achieved by maintaining identical initialization parameters save for the initial CCN concentration in the simulations; we therefore deduce from the simulated results the effect of differing aerosol concentrations on the formation of precipitation. As is expected, increased initial aerosol content leads to delayed drizzle onset due to the effects of aerosol described in the introductory chapter. Further analysis is presented in a case-by-case manner. Finally, we compare the relationships between the retrieval parameters, and show that the effects of drizzle formation on radar reflectivity and optical depth are sufficient to identify drizzling regions in the marine stratocumulus system.

Before all this analysis is performed, of course, we must first describe generally the nature of the simulations being performed. The Nicholls (1984) (hereafter referred to as N84) study of marine stratocumulus clouds represents one of the most comprehensive analyses available to researchers of the genre. Consisting primarily of data obtained by the C-130 aircraft operated by the United Kingdom Meteorological

Research Flight (UKMRF) during a field campaign over the North Atlantic on 22 July, 1982, the N84 study serves as a convenient comparison case for the LES modeller wishing to verify model runs with in-situ cloud observations of real marine stratocumulus clouds. Khairoutdinov (1998) verified the original version of the CIMMS LES model using the N84 test (as well as data from the ASTEX experiment) as a reference case. Here we reproduce these earlier results applying the present version of the model to an STBL case using initialization parameters that simulate the N84 study. We also compare the modelled results so obtained with the in-situ measurements made by the UKMET team and described in Nicholls (1984).

3.1 Background and Motivation

The thrust of the N84 study was to be the first truly comprehensive sampling of PBL-topped marine stratocumulus clouds. This ambitious approach was undertaken due to the relative dearth of information available to researchers of marine stratocumulus at that time, and has provided a great deal of information about PBL-topped marine stratocumulus clouds, especially in regards to cloud microphysics and boundary layer dynamics associated with these clouds. As a comprehensive case study, complete environmental conditions were recorded during the N84 case, and where applicable, these environmental parameters were used in the initialization of the CSU-CIMMS model run used here.

Since the CIMMS model initialization procedure has changed little throughout the evolution of the model over the years, it was simple to apply the N84 initialization parameters as described by Khairoutdinov (1998) with minor modifications to the

initial aerosol properties. Again, the model was initialized, as in Khairoutdinov (1998) on a 40x40x50 grid, with grid resolution of 75 meters in the horizontal and 25 meters in the vertical. This translates to a modelled domain of 3 kilometers in the horizontal and 1.25 kilometers in the vertical. The dynamical time step for the model was 3 seconds, with microphysics code executing on a time step of 0.1 seconds. The total model run consisted of 3,600 time steps, or three hours of modelled time. The initialization sounding consisted of four points, representing a subcloud mixed layer, the cloud layer itself, and a strong inversion level at about 800 meters. Figure 3.1 shows the initialization sounding for the model run. No deviation from geostrophy was included in the initialization parameters. This profile was selected to match the initial conditions prevalent during the N84 case.

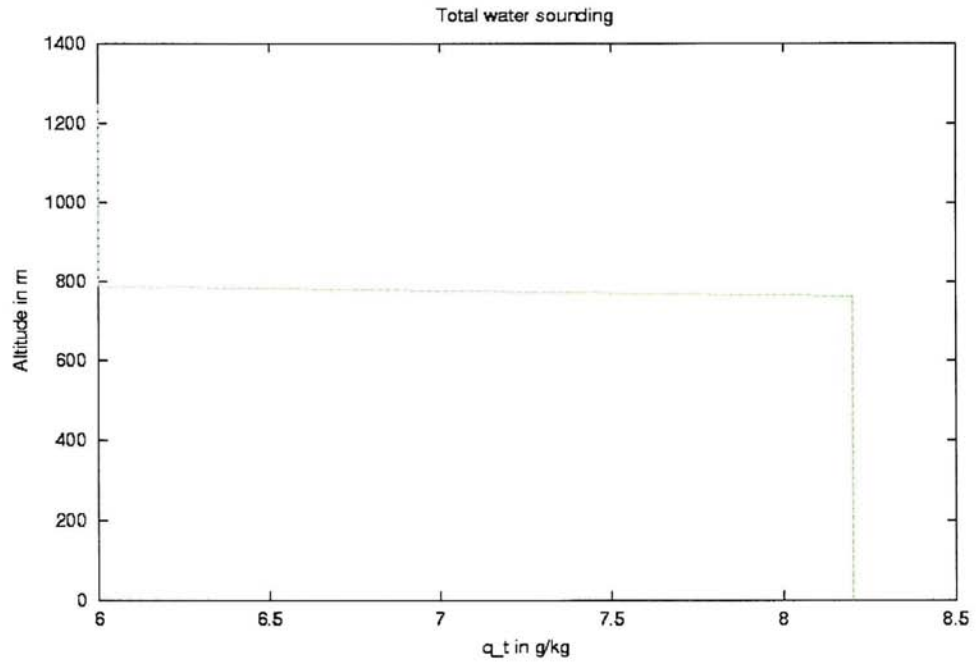
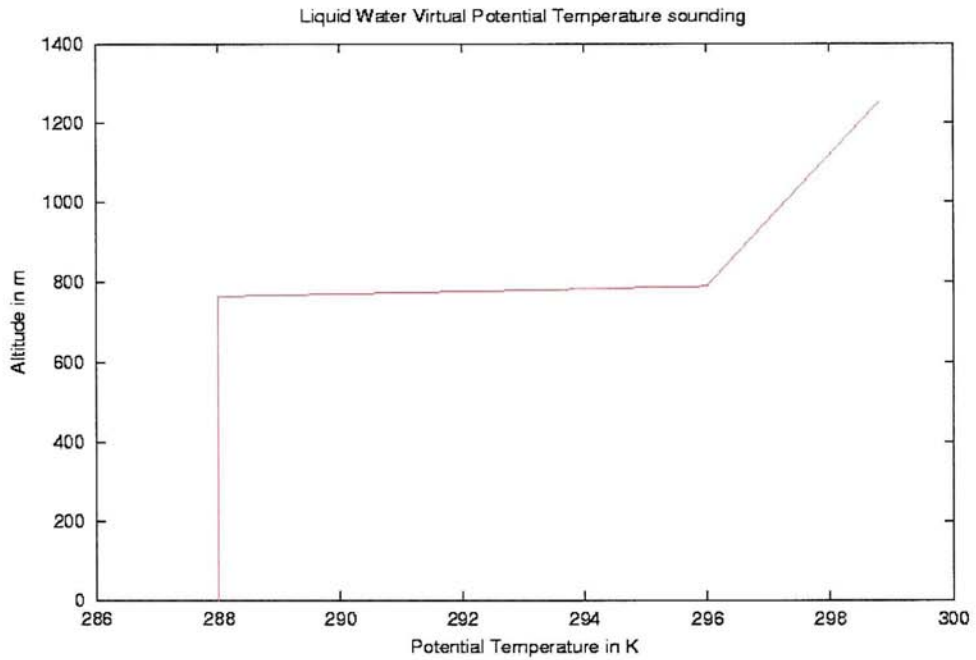


Figure 3.1. Initialization sounding for the Nicholls (1984) case. Liquid-water virtual potential temperature sounding in red, water mixing ratio in green. Temperature is measured in degrees Kelvin, mixing ratio is specified in grams of water per kilogram of air.

Several other parameters were specified as initial conditions: cloud-top fluxes of shortwave and longwave radiation in the CSU-CIMMS LES are set by specifying the zenith angle passed to the radiation code routine; the zenith angle was set to reproduce shortwave and longwave cloud-top fluxes of 860 and 276 W/m², respectively. The surface heat and moisture fluxes were specified as 0.1 and 1x10⁻⁵ K*m/sec², respectively. The surface roughness length was set at 0.0002 m. The large-scale subsidence was set at 5x10⁻⁶ sec⁻¹. The microphysical initialization parameters (including aerosol amounts and types) were specified in the bulk microphysics code, and are described by Khairoutdinov and Kogan (2000.) In brief, the aerosol used consists of ammonium bisulfate aerosol with user-specified initial CCN concentrations.

3.2 'Clean' Model Run

The first model run completed used the initialization parameters described above, with an initial aerosol concentration of 50 cm⁻³. This closely replicates the results of the Khairoutdinov (1998) paper, where initial aerosol concentrations were 45 cm⁻³. This concentration represents a 'clean' marine environment, as is found over non-polluted sections of the ocean. The microphysical structure of such a cloud would be expected to have relatively low cloud-droplet number concentration, as the availability of CCN aerosol for droplets to nucleate is small. Also, one would expect larger drizzle droplet sizes, as collision-coalescence would dominate once the drizzle process begins. Modelled results are presented in section 3.2.a

3.2.a Modelled Results

Plots of the time/spatially averaged model output profiles of selected quantities are compared to the Nicholls (1984) data in Figure 3.2. With the exception of the w^2 quantity, agreement is reasonably good with the Nicholls data, as is expected, considering that this model is tuned to the type of cloud Nicholls observed. (Incidentally, there is a large spread in the measured values of w^2 in the Nicholls data, and other simulations of this case have produced similar discrepancies in this field, (e.g. Khairoutdinov, 1998.))

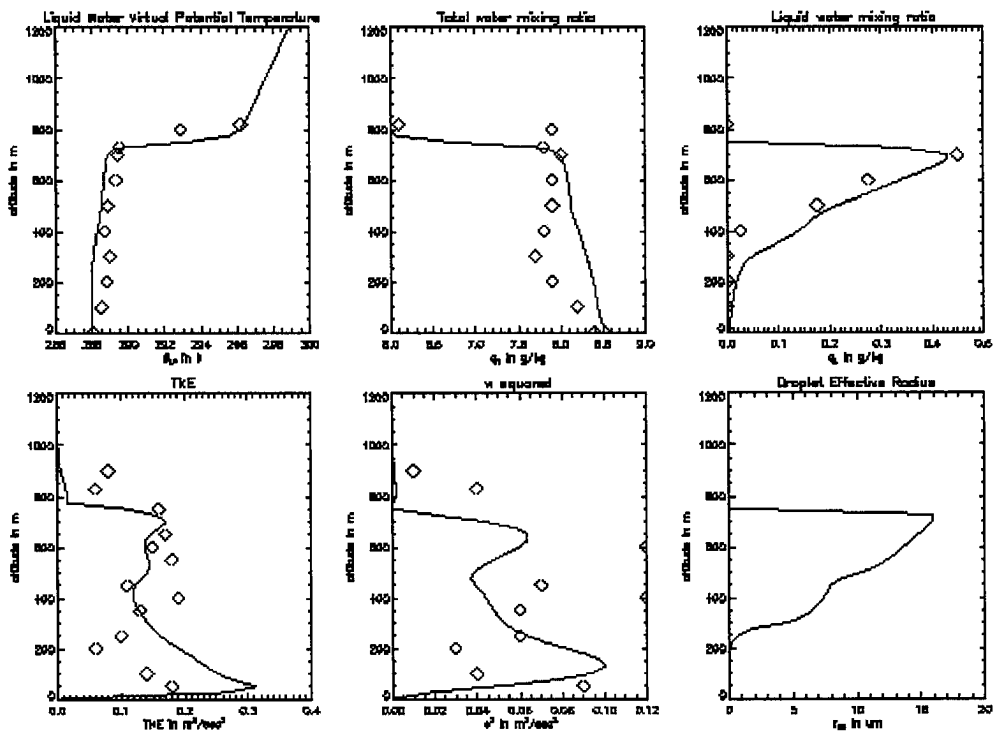


Figure 3.2. Six-panel plot showing comparisons of the Nicholls (1984) measured data with the ‘clean’ model run of the CSU-CIMMS LES model. Nicholls data is represented by symbols, while model output is represented by solid lines.

The model initializes with a ‘perfect’ horizontally homogeneous marine stratocumulus cloud, and within a short period, evolves this cloud into a more realistic

marine stratocumulus system with horizontal variability. Radar reflectivities derived from using properties early in the simulation are on the order of -15 dBZ, with cloud optical depths of approximately 17.5. The cloud evolves for roughly 27 minutes modelled time before initiating the drizzle process. During this 'no-drizzle' phase, the cloud contains as much as 0.6 g/kg of cloud water. It is important to note that coalescence is allowed from the very first time step - there are no numerical constraints on the model governing the drizzle initiation process. This is to ensure that the cloud microphysics are as accurate as possible - crucial for the radar reflectivity retrievals - as forcing the cloud to remain in a non-drizzling state would likely result in artificially inflated cloud droplet radii. This, of course, would dramatically skew the cloud radar reflectivity data to much higher values. By letting the cloud 'choose' when the drizzle process is to initiate, radar results are ensured to be as accurate as possible, as well as providing insight into the drizzle-formation process.

After 27 minutes of modelled time, the cloud begins to produce precipitation. This is signalled by the initial presence of drizzle water in the model's partitioned microphysical scheme. From this point on, radar reflectivity in the cloud is dominated by the drizzle signal - computed cloud reflectivities remain in the -15 dBZ range, while the drizzle signal reaches as high as +10 dBZ. Computed rainrates are slightly below 1mm/day, which agrees well with rainrates noted in other studies of these cloud systems, e.g. Khairoutdinov (1998.) The rainrate is computed using the prognosed drizzle mixing ratio in the Marshall-Palmer dropsize-distribution. After approximately 84 minutes of modelled time, the cloud becomes convective and

begins to decouple somewhat from the surface moisture layer, as evidenced by the decrease in water vapor mixing ratio at around 400 meters. The convection is thought to be driven by updrafts/downdrafts generated by precipitation, while the decoupling is thought by the model's author to be an artifact of the radiation scheme, which does not modify the zenith angle of incident solar radiation as would be expected from the changing position of the sun during the day. A test run of the model, performed without shortwave incident radiation, did not produce any convection or decoupling, which supports the argument that the non-realistic, long-term exposure to solar radiation is the cause of the cloud decoupling. Other potential sources of decoupling include wind-shear generation of turbulent kinetic energy, or cloud-top entrainment instability; in this case, the wind shear is likely insufficient to generate the necessary kinetic energy ($u_g < 5$ m/sec) and the initial profile is prone to CTEI according to both the Lilly (1968) and the Randall-Deardorff (1980) CTEI criterion. This was verified by computing the difference between equivalent potential temperature just above cloud top and the equivalent potential temperature immediately below cloud top. This difference was positive, satisfying the Lilly (and by default, the more stringent Randall-Deardorff) criterion for stability to cloud-top entrainment. These results also suggest the dominant role of solar radiation in the genesis of cloud decoupling - as such, cloud data is not analyzed for retrieval purposes after this time period, as the microphysics of a convective stratocumulus/cumulus cloud system can differ somewhat from the simple marine stratocumulus cloud, due to convective updrafts. This leaves us with ~40 minutes of simulated drizzle data to work with, which is sufficient for the required analysis.

3.2.b Radar Reflectivity results

Using the methods described in Chapter 2., the radar reflectivity is computed separately for the cloud and drizzle components of the cloud. A representative vertical 'slice' of the radar reflectivity is presented in Figure 3.3, and shows a cross-section (at $y=1.5\text{km}$) of the drizzle and cloud components of the reflectivity. This particular slice is taken from the one-hour mark of simulated model time, approximately 33 model-minutes having passed since the initiation of drizzle in the model.

Note the disparity in the radar reflectivities of the two images: the maximum reflectivity values in the cloud figure are around -15 dBZ, while the maximum reflectivity values in the drizzle figure are nearing +10 dBZ. This difference is emphasized in the Figure 3.3, which contains a time-evolution of horizontally-averaged computed radar reflectivity.

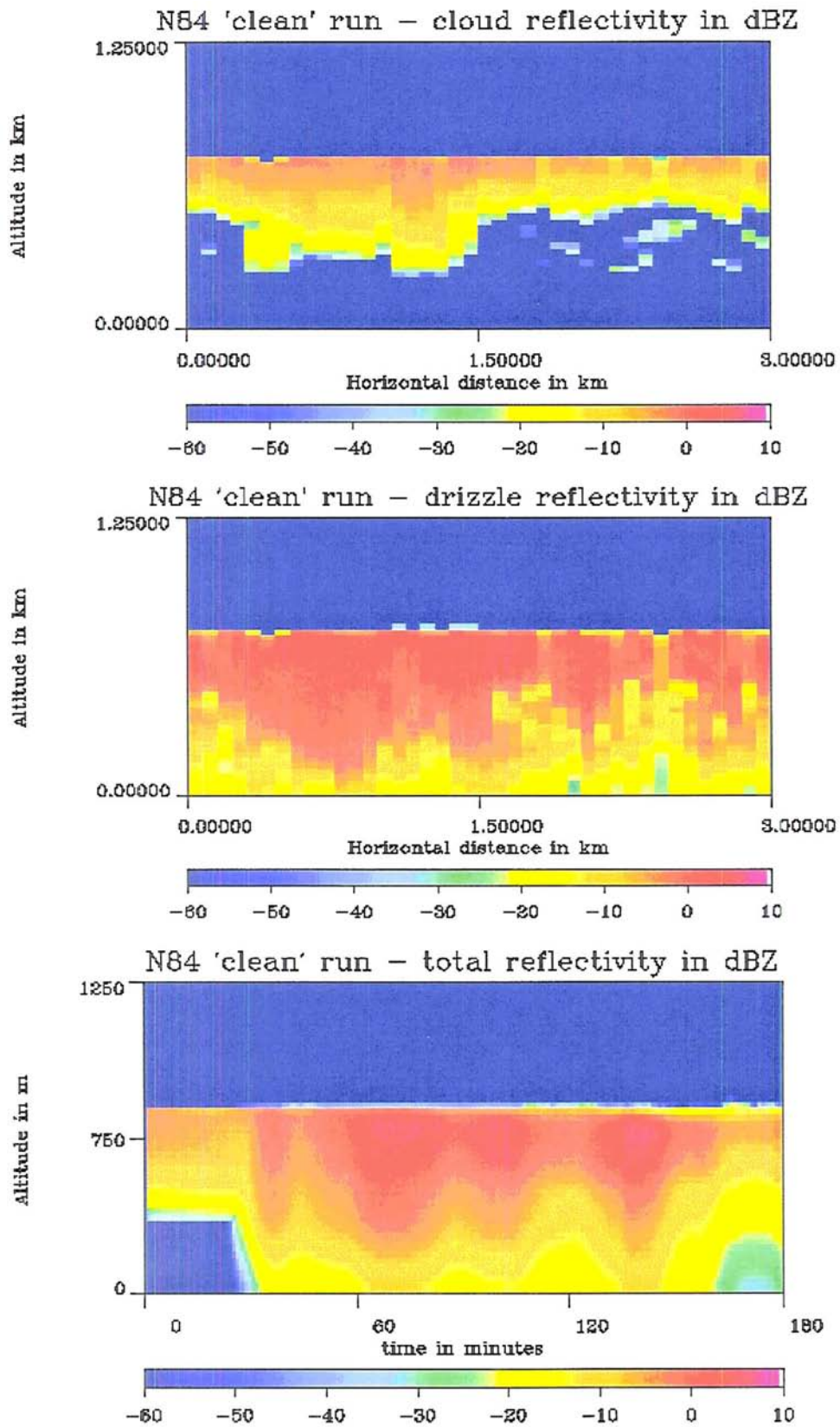


Figure 3.3. Radar reflectivity cross sections. The cloud and drizzle reflectivities are taken at $y=1.5$ km and $t=60$ minutes, while the total reflectivity is horizontally averaged. Units in dBZ.

As the simulation progressed, the cloud component of the liquid water decreased as a result of drizzle production, as is expected. This is seen in the simulation as a gradual decrease in the thickness of the cloud radar reflectivity in favor of the drizzle radar reflectivity.

Figure 3.4 presents a probability-density function (PDF) of total radar reflectivity for the non-drizzling and drizzling segments of the cloud evolution. We see evidence of the separation of drizzle radar reflectivities (at around -10 dBZ) and cloud reflectivities (at around -25 dBZ) as is described in Baedi, Boers, and Russchenberg (2001). The secondary maximum of cloud reflectivity at around -10 dBZ is thought to consist of ‘pre-drizzle’ large cloud droplets that have yet to undergo the autoconversion process – and as such, are representative of an artifact of the cloud microphysical scheme.

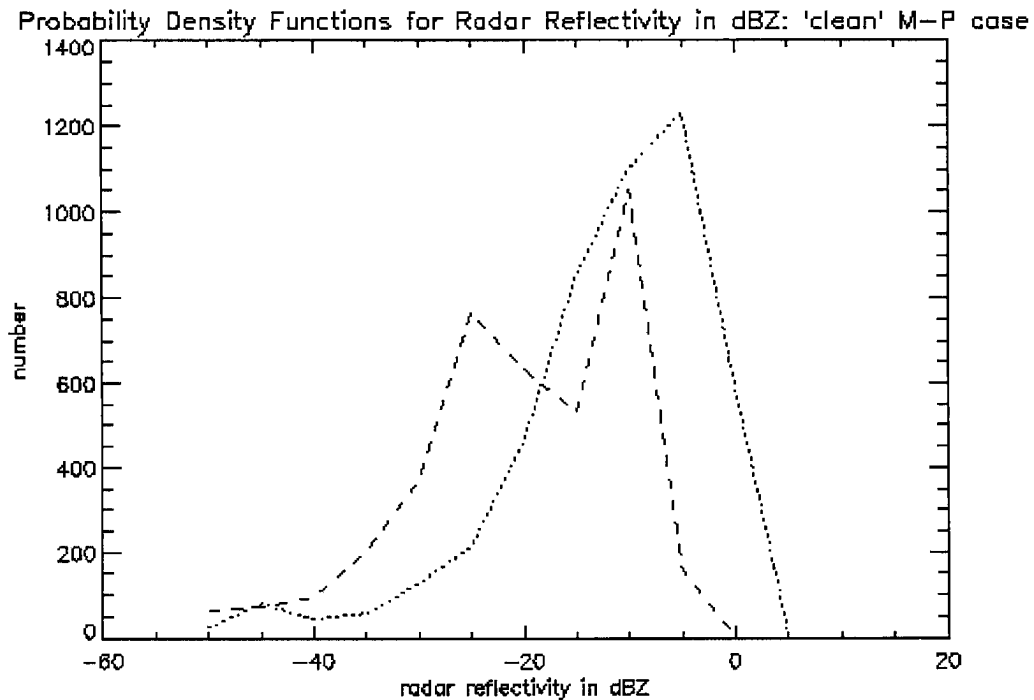


Figure 3.4 Probability-density function of total radar reflectivity for the ‘clean’ simulation. The dotted line represents the drizzle portion, while the dashed line represents the non-drizzling portion of the cloud evolution.

3.2.c Cloud Optical Depth

Figure 3.4 presents evolution of the mean cloud optical depth throughout the 'clean' simulation. Cloud optical depths begin with a value of 17.6 and decreases to final values of around 5 at the end of the non-convective drizzle segment of the run. This optical depth includes both the cloud and drizzle components.

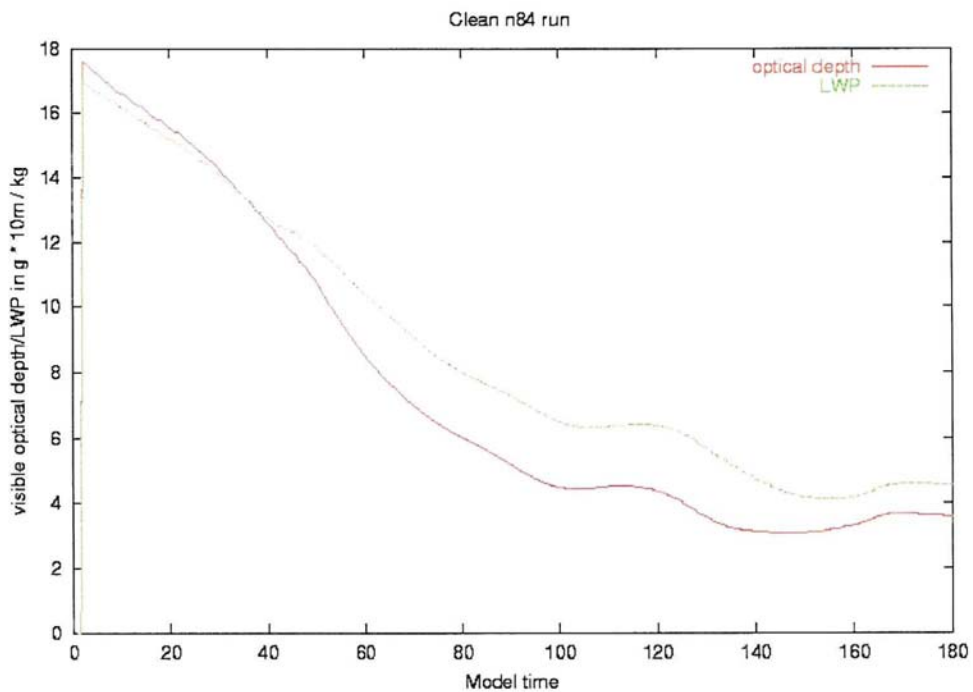


Figure 3.4. Visible optical depth and liquid water path as a function of time in the model. Time is in minutes.

3.3 'Dirty' Model Run

The second model run performed was, for all practical purposes, a duplicate run of the 'clean' case, with the single exception of an initialized ammonium bisulfate aerosol concentration of 150 cm^{-3} . This simulation provides a test of the effect of

aerosol (expressed as CCN) on the microphysical evolution of the cloud structure. One would expect the increased CCN to lead to an increase in cloud droplet number concentration, while reducing the mean cloud droplet radii, as water vapor would preferentially nucleate the CCN rather than condense on available water droplets. This indeed was observed in the simulation, as is shown in Figure 3.5, which compares the cloud number concentration of this simulation to the ‘clean’ simulation.

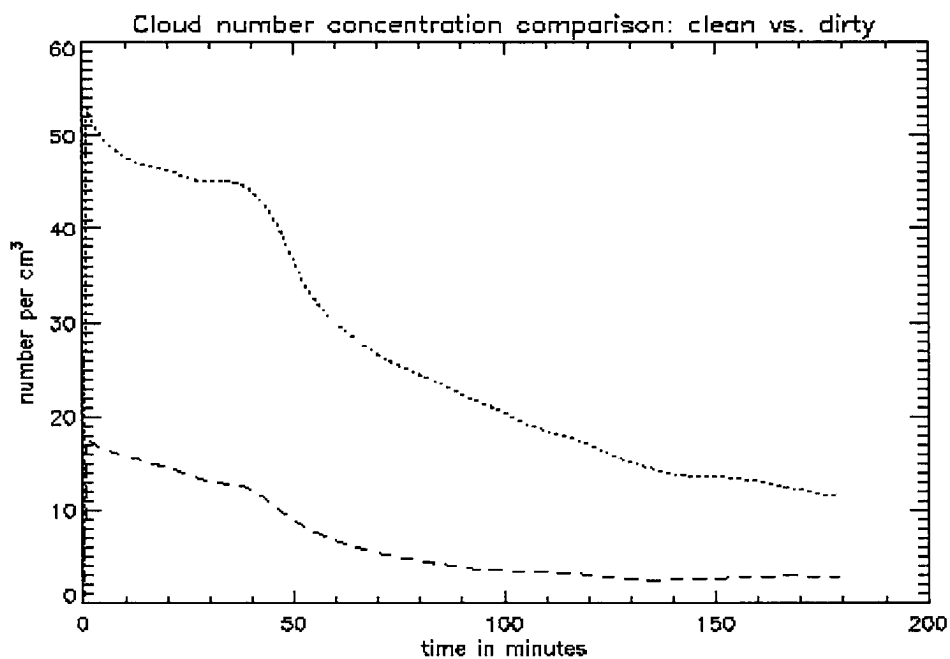


Figure 3.5. Spatially-averaged cloud droplet number concentration comparison between the ‘clean’ simulation and the ‘dirty’ simulation. The dashed line represents the ‘clean’ simulation, while the dotted line represents the ‘dirty’ simulation.

The effect of increased CCN on drizzle is noteworthy, as drizzle was not initiated until nearly an hour of modelled time, and the drizzle produced was less influenced by the collision-coalescence process, leading ultimately to a greatly reduced drizzle reflectivity component.

3.3.a Modelled Results

Figure 3.6 presents profile comparisons of the simulated data with the Nicholls observations. Agreement with the Nicholls experiment is not as close as the clean case; most notably, there are deviations in the TKE and w^2 plots. However, there is reasonable agreement between the liquid water potential temperature comparison, as in the total- and liquid-water mixing ratio comparisons.

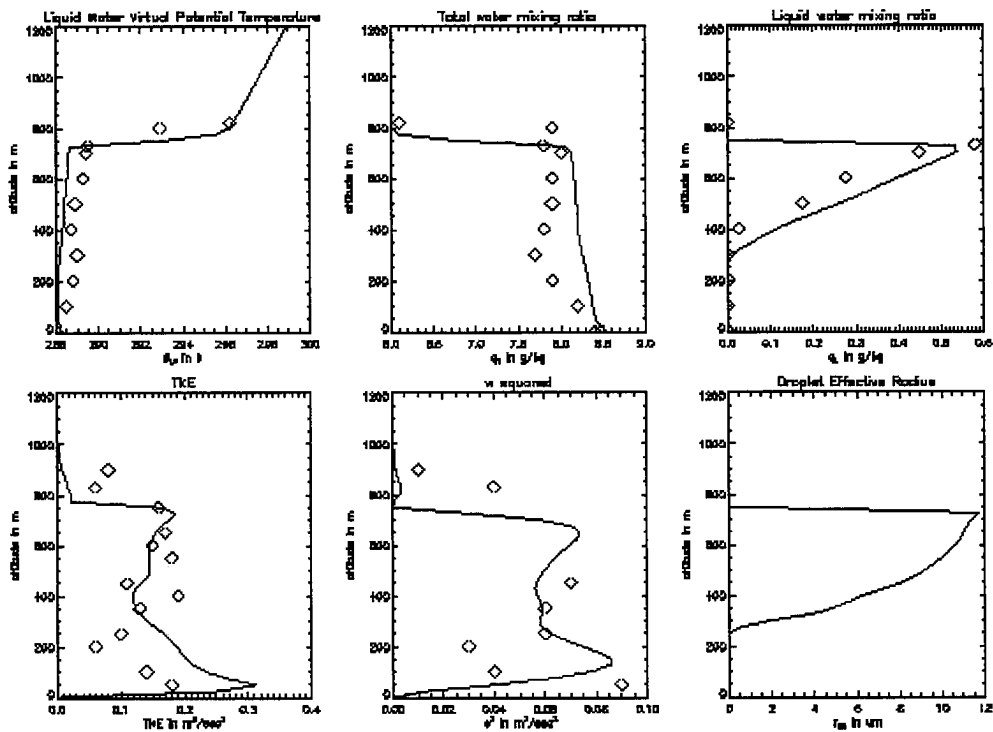


Figure 3.6. Six-panel plot showing a comparison between the ‘dirty’ model run of the CSU-CIMMS LES and the Nicholls (1984) test case. The Nicholls data is represented by symbols, the model run by solid lines.

Again, the model simulation initialized with a ‘perfect’ horizontally homogeneous cloud before evolving into a more realistic-looking system after about $t=10$ minutes of simulated time. This non-precipitating segment of the simulation lasted for nearly one hour of modelled time, during which, there was no formation of drizzle. Cloud droplet number concentrations for this case were, on the average, much higher than

for the ‘clean’ case. Overall, cloud droplet effective radii increased somewhat, during this time period, and the cloud thinned marginally as a result. Also of note is that this simulation was more resistant to convection than the previous run, although signs of some convective activity began to appear near the very end of the run. It is possible that the vertical fluxes set up by precipitation in the ‘clean’ case may have enhanced the ability of convection to form, while the relative dearth of precipitation in this case may have staved off convection during the modelled time period.

The first hint of drizzle precipitation began near $t=69$ minutes. However, the microphysics involved in the formation of this drizzle was noticeably different than the clean case. For this case, the drizzle mass was smaller, and the mean drizzle volume radii were dramatically smaller for this case when compared to the ‘clean’ case. Maximum drizzle droplet volume radii in the ‘dirty’ case were on the order of $\sim 45 \mu\text{m}$, compared to $\sim 50 \mu\text{m}$ in the ‘clean’ case. This reduction in the size of the precipitation droplets, combined with a two-order-of-magnitude decrease in drizzle number concentration led to a drastic decrease in radar reflectivity, as discussed below in section 3.3.b The drizzle produced in this model simulation is presumed to be due to the weakening of the collision-coalescence process, as a result of the smaller cloud droplets. The drizzle droplet number concentration is proportional to inverse one-third power of the mean droplet ration, as well as the autoconversion of drizzle liquid water, which is in turn, seen to vary as the inverse one-third power of the cloud number concentration as shown by the autoconversion equation in the model:

$$\begin{aligned} \left(\frac{\partial q_r}{\partial t}\right)_{auto} &= 2.2q_c^{7/3}N_c^{-1/3}, \\ \left(\frac{\partial N_r}{\partial t}\right)_{auto} &= \frac{\left(\frac{\partial q_r}{\partial t}\right)_{auto}}{\left(\frac{4\pi\rho_w}{3\rho_a}r_o^3\right)} \end{aligned} \quad (3.1)$$

A decrease in cloud droplet size will lead to a decrease in both number concentration and water content of the modelled precipitation. This is as expected, and the above equations were formulated by the model's author using numerical regression of microphysical parameters obtained from an explicit-microphysics LES model simulating the N84 case. (Khairoutdinov and Kogan, 2000.)

3.3.b Radar Reflectivity Results

Figure 3.7 shows a representative cross section of the cloud and drizzle reflectivity, much in the same manner as Figure 3.3. For this simulation, the reflectivity values are roughly the same for both precipitation and the cloud water components.

For this case, average radar reflectivity values hovered around -10-15 dBZ, irrespective of the drizzle component. In fact, the simulation generally produced gridpoints in which the cloud reflectivity frequently *exceeded* the drizzle reflectivity. This is understandable, as drizzle mean volume radii were only on the order of 38 μm ; even with the tenfold increase in radii over the cloud droplet, the number concentrations of initiated drizzle were several orders of magnitude less than the cloud droplets. Essentially, the increase in radar reflectivity due to the formation of large size drizzle drops is negated by the relative scarcity of these drizzle drops.

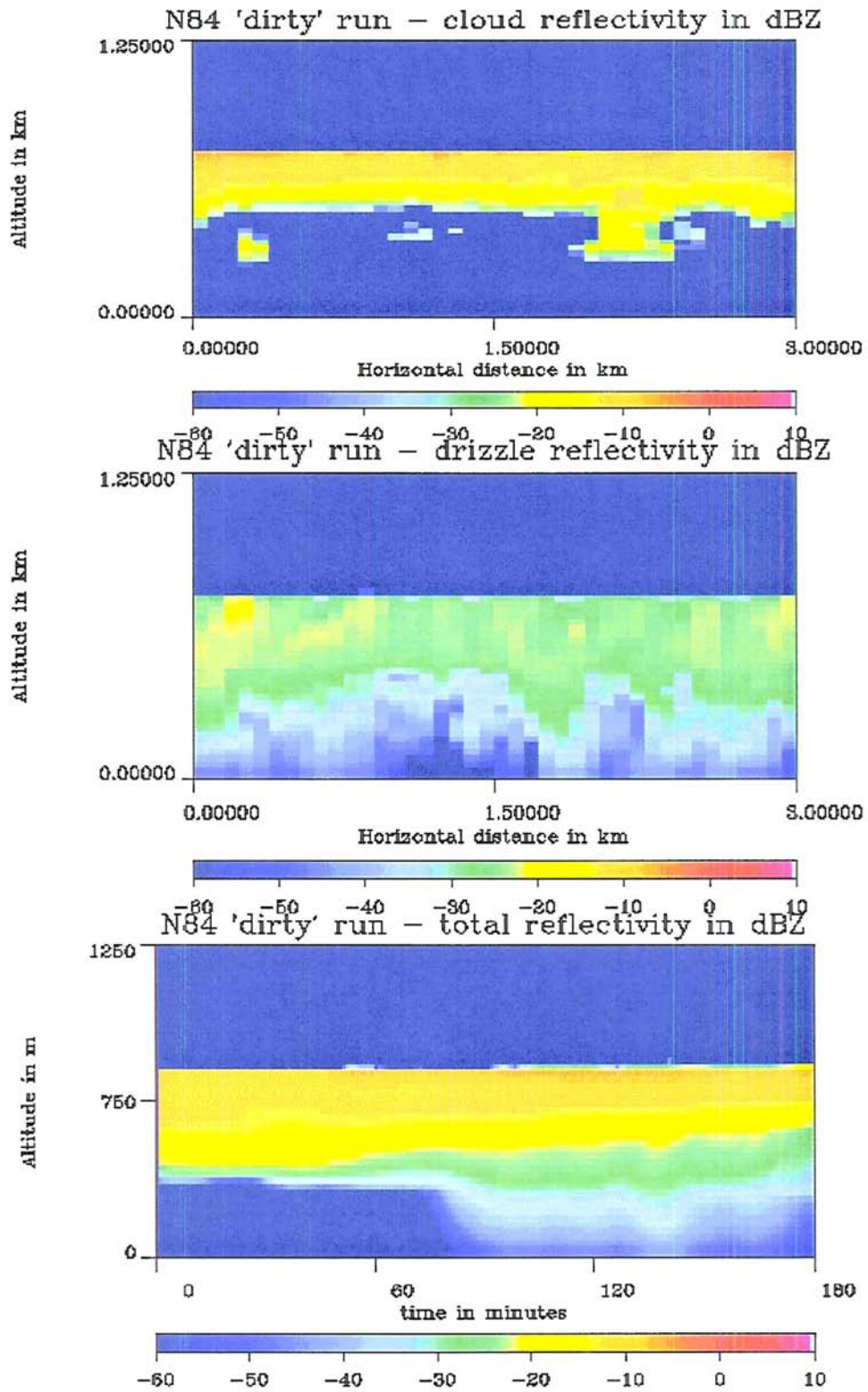


Figure 3.7. Radar reflectivity cross sections. The cloud and drizzle reflectivities are taken at $y=1.5$ km and $t=120$ minutes, while the total reflectivity is horizontally averaged. Units in dBZ.

The situation described above would present a distinctly difficult situation for a radar-only, Z-LWC remote sensing retrieval as the bulk of the reflectivity signal here is due to the cloud, and not the drizzle. For our purposes, however, we have an ideal case to study the effects of drizzle formation, as our retrieval processes some information about the droplet radii. As such, the large drizzle droplets produced in this simulation (albeit at extremely small number concentration) should produce a noticeable effect in the retrieval output.

Figure 3.8 presents a PDF of the radar reflectivity for the ‘dirty’ simulation, again partitioning the drizzle and non-drizzle elements. Note that the cloud reflectivity peak is higher than the computed drizzle reflectivity peak. Also of interest are the precipitation modes exhibited by the drizzle signature – two distinct reflectivity peaks exist. This is thought to represent the spatial variance in droplet size for the cloud – larger, higher reflectivity drops reside near cloud top, while smaller droplets reside in the lower regions of the cloud. Given the extremely low contents of drizzle produced in this simulation, it is difficult to draw comparisons between this simulation and the ‘clean’ simulation, especially in respect to the drizzle and cloud reflectivity components. However, we do see in the ‘dirty’ simulation evidence that cloud reflectivity peaks at around -10 dBZ, which further supports the analysis of Baedi, Boers, and Russchenberg (2001) as well as our own theoretical analysis presented in Chapter 2.

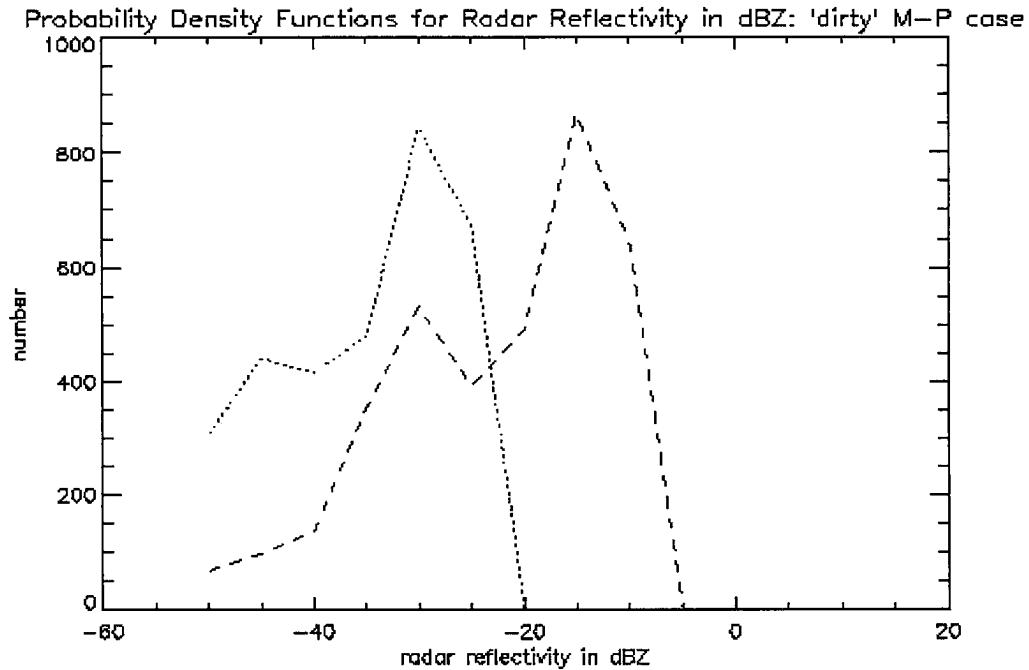


Figure 3.8 Probability-density function of total radar reflectivity for the 'dirty' simulation. The dotted line represents the drizzle portion, while the dashed line represents the non-drizzling portion of the cloud evolution.

3.3.c Cloud Optical Depth

Figure 3.9 shows a time-evolution plot of the visible optical depth and liquid water path for the 'dirty' simulation. Optical depths are higher than in the clean case, as the number concentration of cloud droplets is higher for the same given liquid water path. Also, the optical depth remains higher for a longer period of modelled time, as precipitation does not appear in the simulation until approximately $t=69$ minutes. Optical depths start with values of roughly 25, and drop off to a minimum value of roughly 8 or so at the end of the simulation.

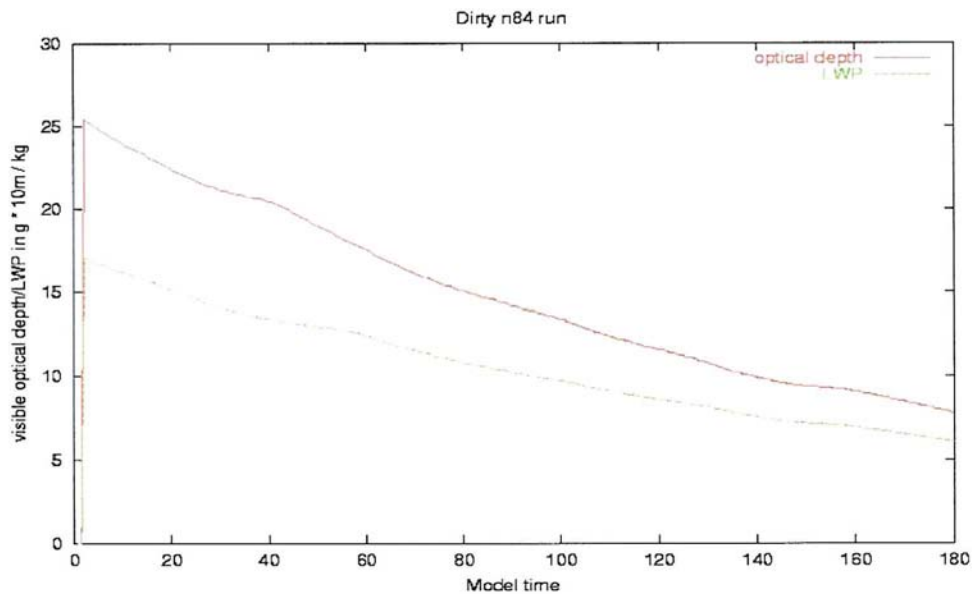


Figure 3.9. Visible optical depth and liquid water path as a function of time in the model. Time is in minutes.

3.4 ‘No Drizzle’ Model Run

The radar reflectivity/optical depth retrieval described in Chapter Four is designed to sample marine stratocumulus clouds that do *not* contain drizzle. As such, it would be instructive to perform a simulation during which no drizzle is initiated by the model. Such a simulation would allow us to better examine the effects of drizzle on the retrieval, as we have a non-drizzling comparison case with which to contrast the drizzling simulations.

This simulation uses the same initialization parameters as the ‘dirty’ run, but increases the initial CCN to 300 cm^{-3} , does not allow the autoconversion of drizzle from cloud water to begin, and does not allow sedimentation of larger cloud droplets. This extremely high initial CCN count is specified so as to ward off the non-physical effects the model produces as cloud droplets grow to sizes where they would normally

undergo autoconversion. The model results, therefore, are not entirely what one would expect from a real, physical cloud, but are instructive and provide a means of exploring the relationship between radar reflectivity and visible optical depth in a non-drizzling marine stratocumulus cloud. This case is also not entirely unrealistic as it represents the case of *extremely* high CCN concentrations, as might be found off a highly-polluted coastline.

3.4.a Modelled Results

Figure 3.10 shows the familiar six-panel comparison of the modelled results as compared to the Nicholls (1984) data. Surprisingly, the simulated data are not as different from the observed data as one might expect: while there exist deviances in the turbulent kinetic energy profile, the rest of the comparisons seem reasonable.

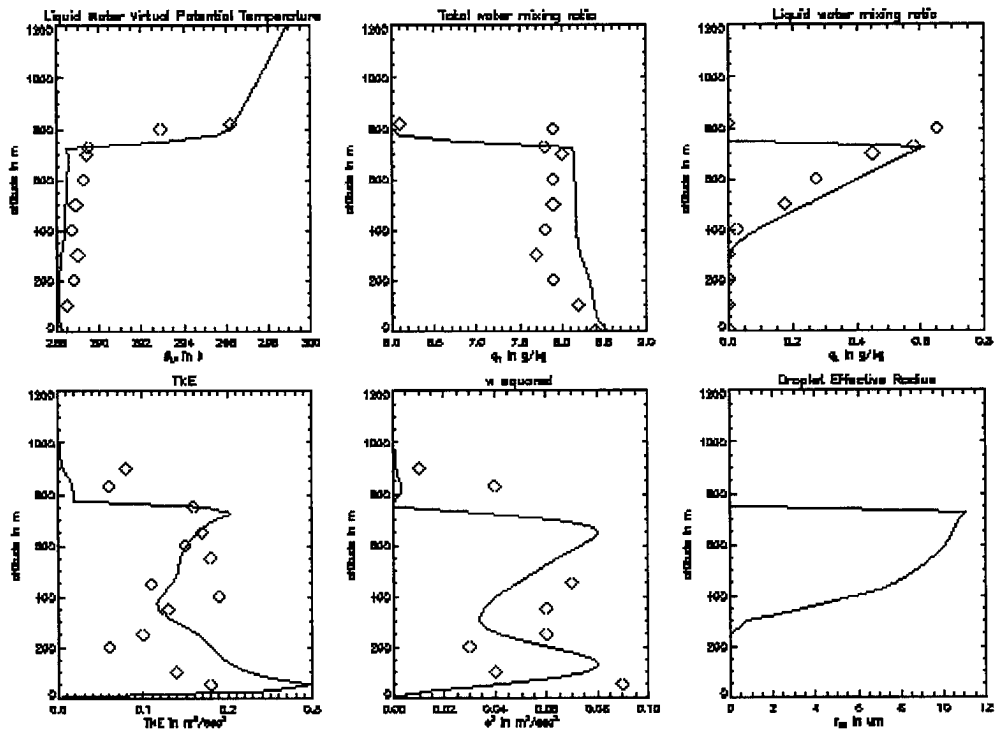


Figure 3.10. Six-panel plot showing a comparison between the ‘no drizzle’ run of the CSU-CIMMS LES and the Nicholls (1984) measurements. The Nicholls data is represented by symbols, while the modelled output is represented by solid lines.

As with the ‘dirty’ simulation, this simulation appeared to generate little convective activity near the end of the model cycle; most likely due to the complete lack of precipitation to force vertical updrafts and downdrafts. Moderate decoupling at $z=300\text{m}$ is somewhat in evidence, and the evolution of the cloud supports the notion that the cloud eventually separates from the surface moisture, as the cloud continually thins as the cloud evolution progresses.

As in the previous two cases, the initial few minutes of the simulation are of a perfect, horizontally homogeneous cloud system. Throughout the entire evolution of the cloud, very little changes in the gross structure of the cloud system, and the horizontal structure of the cloud remains relatively homogeneous. Average values of cloud liquid water are relatively similar to the ‘clean’ case, although the cloud droplet effective radii are marginally smaller, with maximum values of approximately $11\ \mu\text{m}$. As the cloud evolves, the cloud-top height increases, and the overall depth of the cloud decreases, likely a result of the eventual slow decoupling of the cloud system.

3.4.b Radar Reflectivity results

Figure 3.11 shows the familiar radar reflectivity cross section. The drizzle reflectivity is also shown, although at no point in the model run does drizzle become manifest.

The reflectivity cross-sections are taken at $t=60$ minutes, mirroring the ‘clean’ case figure. For this case, maximum radar reflectivity values were around $-5\ \text{dBZ}$, with mean values more representative of the cloud of $-15\ \text{dBZ}$ in frequent evidence. Higher values of radar reflectivity positively correspond to the largest cloud droplets.

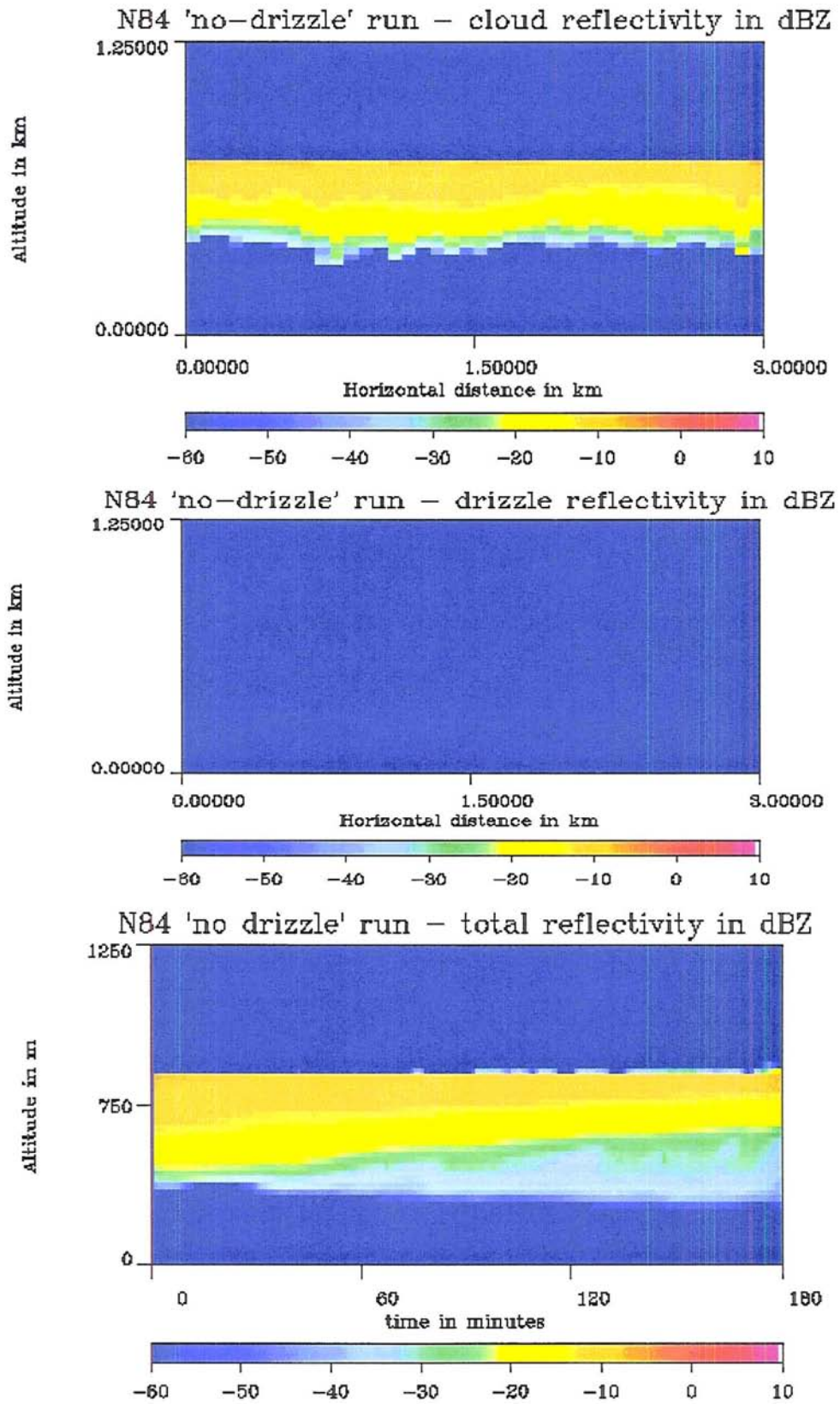


Figure 3.11. Radar reflectivity cross sections. The cloud and drizzle reflectivities are taken at $y=1.5$ km and $t=60$ minutes, while the total reflectivity is horizontally averaged. Units in dBZ.

Maximum radar reflectivity values were around -5 dBZ, with mean values of cloud reflectivity observed to be -15 dBZ. A PDF of the radar reflectivity for the 'no drizzle' simulation is provided as Figure 3.12. This figure represents only cloud reflectivity, as no drizzle was produced by the simulation. Again, the maximum frequency of radar reflectivity is seen to be at approximately -10 dBZ, and exhibits a secondary maximum at around -35 dBZ. Finally, we show still more support for the upper-limit of cloud reflectivity as described in our theoretical analysis of radar reflectivity as well as the supposition of Baedi, Boers, and Russchenberg (2001) as again, maximum cloud reflectivity values rarely exceed -10 dBZ in this final simulation.

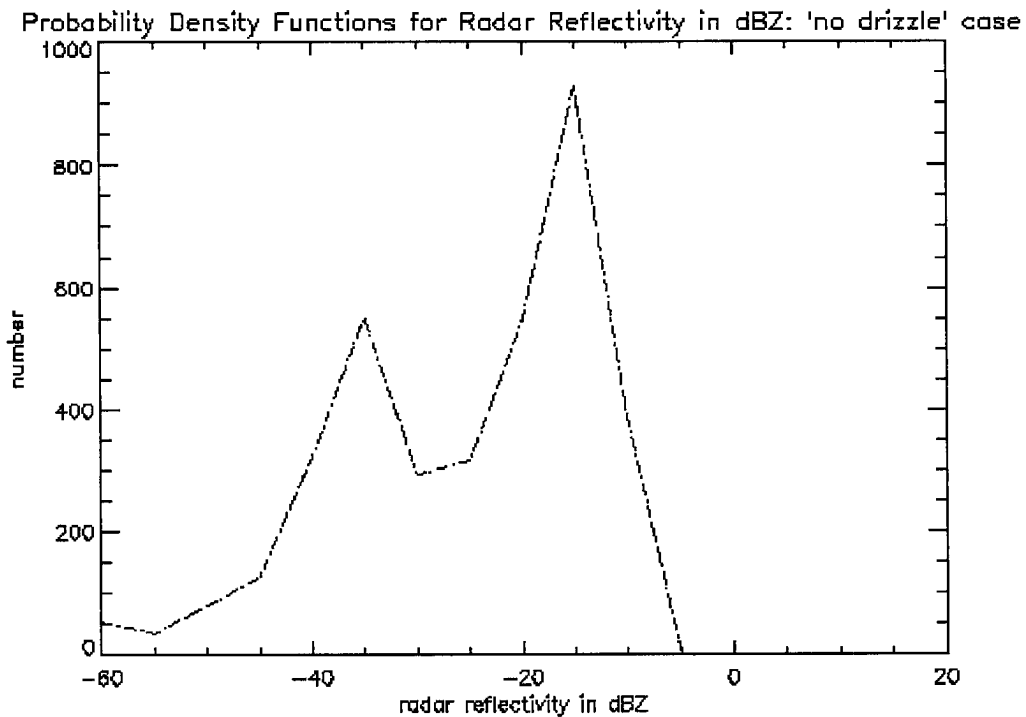


Figure 3.12 Probability-density function of total radar reflectivity for the 'no drizzle' simulation.

3.4.c Cloud Optical Depth

Figure 3.13 shows the time evolution of optical depth for the ‘no drizzle’ run:

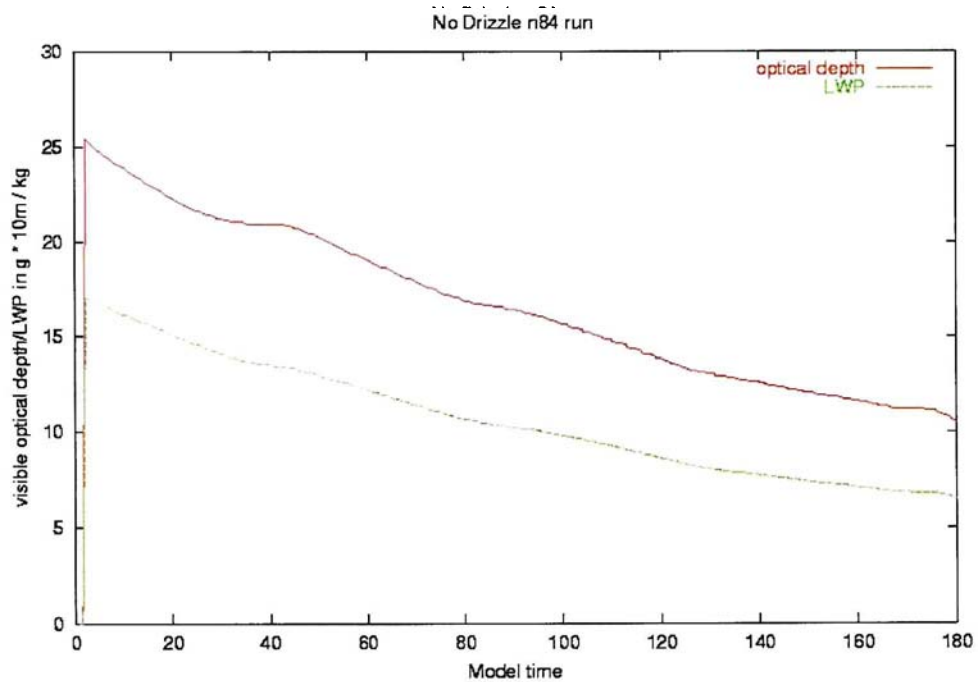


Figure 3.13. Visible optical depth and liquid water path for the ‘no drizzle’ run of the CSU-CIMMS LES

Initial optical depths are roughly the same as the ‘dirty’ simulation, but do not drop as rapidly with time as the run progresses. This is as expected – the entirety of the liquid water path for this cloud is made of nothing but cloud droplets, and as such, the expected optical depths should be much larger than a cloud with a similar LWP containing drizzle droplets. Near the end of the simulation, optical depths decreased to values of 15 or so, in contrast to the ‘dirty’ simulation, which produced final optical depths of roughly 8.

3.5 Discussion

The three simulations presented above show the usefulness of LES modelling of cloud parameters – the computed quantities agree well with observational and theoretical analysis, and as such, we have high confidence in the simulated results. As such, the three simulations presented above may be used to compare observable features with the intent of studying the effects of drizzle on said features. Principally, we are interested in integrated radar reflectivity, cloud liquid water path, and cloud visible optical depth, as these are parameters commonly measured from spaceborne instruments. Figure 3.14, 3.15, and 3.16 present comparison plots between the three simulations of visible optical depth versus integrated radar reflectivity, liquid water path versus integrated radar reflectivity, and liquid water path versus visible optical depth, respectively.

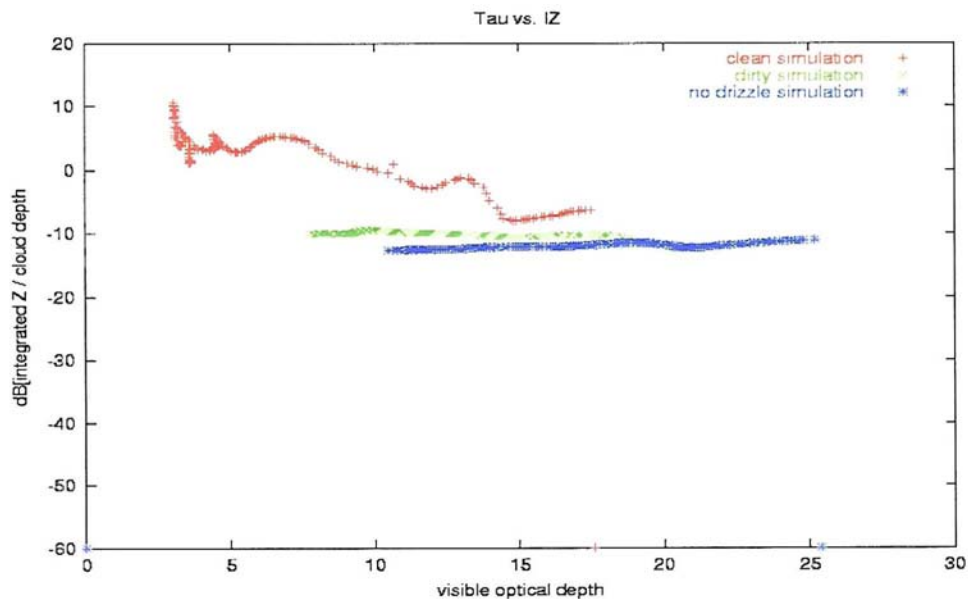


Figure 3.14. Comparison between the three simulations of cloud optical depth versus integrated radar reflectivity.

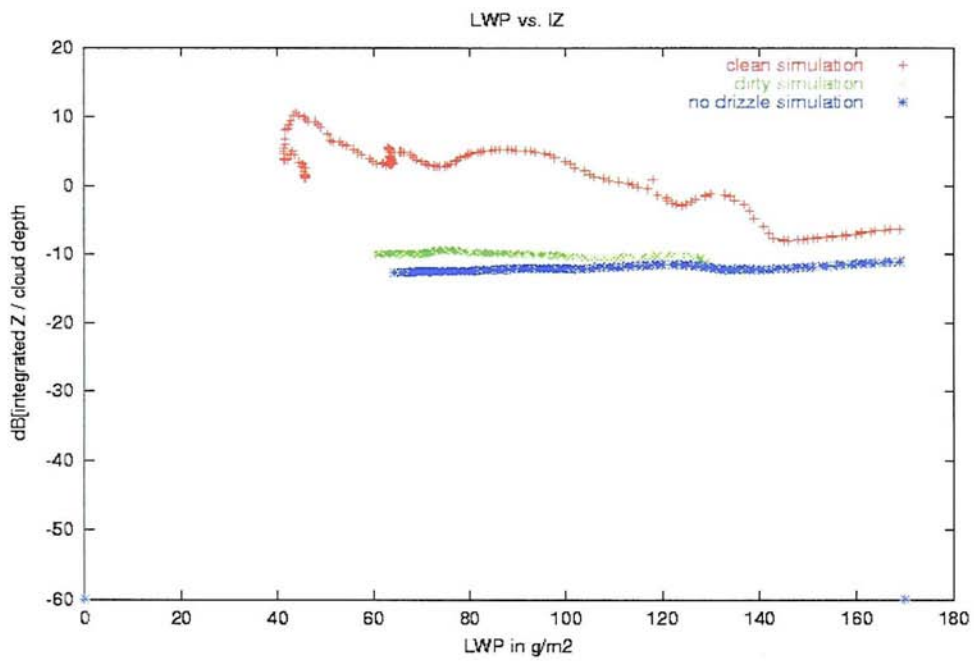


Figure 3.15. As in Figure 3.14, but with LWP versus IZ.

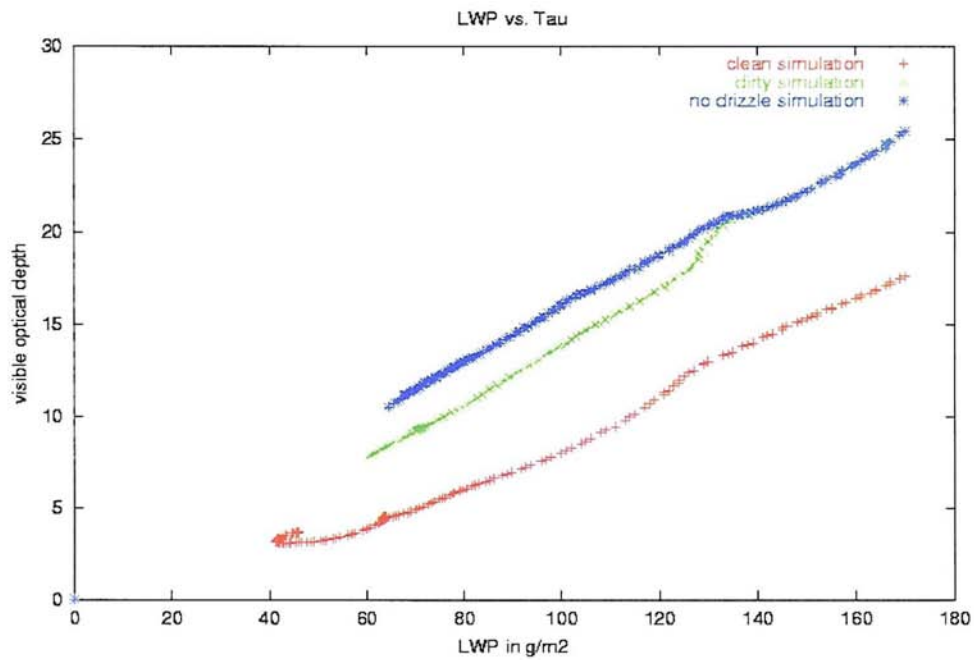


Figure 3.16. As in Figure 3.15, but with LWP versus optical depth.

What we see in the above figures are essentially the difference between the non-drizzling and the heavily drizzling case, as the ‘dirty’ simulation produces results similar to the ‘no drizzle’ case. We do see some separation of the ‘dirty’ simulation from the ‘no drizzle’ simulation after drizzle genesis, shown as a decrease in optical depth and slight increase in integrated radar reflectivity; however, ‘real’ data would exhibit a sufficiently large spread of values due to measurement error so as to wash this slight difference out. What is useful is to draw some generalizations between the obviously non-drizzling cloud simulations and the obviously drizzling simulation. As we see in Figures 3.14 and 3.15, there appears to be a natural separation of mean cloud radar reflectivity at around -10 dBZ, above which the data is generally (although not always, as is seen in Figure 3.4) a drizzle signature, and below which, the data is representative of cloud. Again, this further supports the suggestion made by Baedi, Boers, and Russchenberg (2001) that the radar reflectivities of drizzle and cloud are partitioned around -10 dBZ. We also note the value of adding LWP to potential future retrievals – not only does drizzling stratocumulus exhibit higher reflectivities than non-drizzling systems, the LWP of drizzling systems is lower, as is the cloud optical depth, as is seen in Figure 3.16. This information, combined with the radar reflectivity partitioning found above, might serve as a useful means to identify drizzling and non-drizzling clouds using readily available remotely-sensed parameters. As such, this identification would be of use in future retrieval algorithms where drizzle discrimination is important, such as radar retrievals of cloud microphysical parameters.

The desired result of these simulations is the creation of a comprehensive dataset consistent with measurements of real, physical marine stratocumulus clouds. To the degree possible, these data represent the necessary physical and dynamical structure of the marine stratocumulus system necessary to facilitate computation of realistic radar fields and optical depth. To this end, the simulations were performed to reproduce, as faithfully as possible, the results found both in previous validated runs of the model (primarily the results of Khairoudinov (1998) and Khairoutdinov and Kogan (2000)) as well as empirical measurements from the field.

These simulations reported above serve their purpose well – the modelled results agree reasonably well with previously published observational studies of marine stratocumulus cloud systems. The microphysical parameters produced by the model are not without their own limitations, of course, as variances in the vertical velocity fields were highly dependent on initial conditions for each model run, and the turbulent kinetic energy field for the ‘no drizzle’ run showed higher sub-cloud values than other simulations. However, the cloud parameters measured (especially the number concentration and cloud droplet effective radii) were well within expected values for a realistic simulation of marine stratocumulus cloud systems. Moreover, the optical depth results behaved as predicted: for a relatively constant LWP, the optical depth decreased as expected as the cloud constitution changed from cloud droplets to drizzle droplets. The time evolution of the model behaved in a realistic manner, and the overall results of the simulations, especially for parameters directly used in the retrievals to be described shortly, are sufficiently realistic for further research to be of use.

Chapter 4

On the Relationship Between Optical Depth and Radar Reflectivity of Marine Stratocumulus in the Presence of Drizzle

We present in this chapter an overview of the retrieval used, and apply the simulated results described in Chapter 3 along with the theory presented in Chapter 2 to the retrieval method described presently. After this analysis is performed, we observe that the retrievals of cloud liquid water and effective radius compare favorably to the modelled results for non-drizzling and lightly drizzling cases, and that secondly, for heavy drizzle (such as the ‘clean’ simulation) the retrieval procedure breaks down. We explore further the effects of drizzle on the retrieval method, and for the case where the retrieval fails, we suggest reasons as to the cause of failure, based on assumptions made in the retrieval.

4.1 Background and Motivation

The motivation for studying the parameters described above is quite simple: utilizing multiple parameters in a sophisticated retrieval algorithm produces much more accurate results than does a simple radar-only retrieval (e.g. Sassen *et al.*, 2002.) As such, we seek to use a microphysical retrieval that utilizes more than just radar reflectivity in order to assure greater fidelity in our retrievals of the essential cloud properties.

The retrieval we choose to utilize is described in Austin and Stephens (2000) (hereafter referred to as “Part I”, as this paper is the first of a two-part paper.) The approach utilizes a forward-model applied to the optimal inversion technique (e.g.

Rodgers, 1976) to retrieve three log-normal distributions over radius, number concentration, and standard deviation, thus defining the relevant microphysical parameters of the cloud system. The functional form of the forward model is:

$$\mathbf{y} = \mathbf{F}(\mathbf{x}, \mathbf{b}) + \varepsilon_y \quad (4.1)$$

where \mathbf{x} is the state vector of log-normal parameters to be retrieved, \mathbf{b} a vector of forward model parameters not being retrieved, and \mathbf{y} is the ‘input’ vector of measured quantities, which in this case, are integrated radar reflectivity and optical depth. The forward model relies on *a priori* data of number concentration and cloud radii, collected from a variety of measurements of cloud parameters – thus making the forward model ‘tunable’ for different types of clouds. Obtaining the best possible statistical dataset will give better *a priori* values thereby constraining the retrieval method, resulting in more realistic results. As is noted before, the benefit of a model is that one has definitive knowledge of the cloud microphysical parameters, and can, from that data, compute directly the corresponding radar reflectivity/optical depth relationships, thus removing measurement error, and ultimately leading to improvements in the statistical qualities of the retrieval data. Using modelled data as input for the retrieval allows us to study the products of the retrieval only, without needing to consider the measurement error inherent in “real” data.

As described in Part I, the forward model described above is based on a lognormal size distribution of cloud droplets:

$$N(r) = \frac{N_T}{\sqrt{2\pi}\sigma_{\log}r} \exp\left[\frac{-\ln^2\left(\frac{r}{r_g}\right)}{2\sigma_{\log}^2}\right] \quad (4.2)$$

where N_T is the cloud droplet number density, r is the droplet radius, and r_g and σ_{\log} are as described in Austin and Stephens (2000.) The notable difference here is that the forward model uses a log-normal distribution, while the LES model utilizes a gamma distribution. By using the accepted definitions of the radar reflectivity and the extinction coefficient as a function of droplet size distribution, it becomes possible to define the relevant equations for the retrieval:

$$Z = 64N_T r_g^6 \exp(18\sigma_{\log}^2) \quad (4.3)$$

$$\tau = \int_{z_{base}}^{z_{top}} \sigma_{ext}(z) dz = \int_{z_{base}}^{z_{top}} 2\pi N_T r_g^2 \exp(2\sigma_{\log}^2) dz \quad (4.4)$$

Again, as described in Part I, the forward model $\mathbf{F}(\mathbf{x}, \mathbf{b})$ has the form:

$$\mathbf{F}(\mathbf{x}, \mathbf{b}) = \begin{bmatrix} Z'_{dB_{FM}}(z_1) \\ \vdots \\ Z'_{dB_{FM}}(z_n) \\ \tau_{FM} \end{bmatrix} \quad (4.5)$$

where the discretized solutions for Z and τ are based on equations (4.3) and (4.4) and are described in Austin and Stephens (2000.) Thus, the relevant parameters to be retrieved, using Z and τ as observations, are those parameters that define equations (4.3) and (4.4), specifically, $N_T(z)$, $\sigma_{\log}(z)$, and $r_g(z)$, from which other parameters, such as effective radius and liquid water content may be calculated. Of course, synthesized radar and optical depth values from the above model runs may be fed to

the retrieval as easily as real measurements – the difference is that the retrieved values for effective radius and liquid water content may be directly compared to the modelled values of the same. This allows for direct analysis of the performance of the retrieval.

Finally, we apply the retrieval described above to the simulated results of our study. We seek to show that the retrieved results match the values produced by the model, thus demonstrating the utility of the retrieval. Should the retrieval fail (as it does for the heavy-drizzling ‘clean’ simulation) we seek to describe the failure mechanism of the retrieval. Ultimately, we will hopefully glean from the retrieved results greater insight into the nature of the relationships between observed quantities in the drizzling and non-drizzling marine stratocumulus system.

4.2 Retrieval Results Based on Simulated Data

As the reader will recall, an overall comparison of radar reflectivity and optical depth relationship for the simulated data as well as of CAVEX observations was presented in Chapter Two. We have shown the behavior of the relationship agrees with theory; what is presented here is a case-by-case analysis of the modelled output. This is done primarily to expand upon the details of each simulation with respect to the computed output parameters used in the retrieval process.

Figure 4.1 shows an overall comparison of the modelled radar reflectivities plotted against the model-produced optical depths, similar to Figure 2.3, but omitting the CAVEX observations. Drizzle component is shown in green symbols, while the non-drizzle, cloud-only component is shown in red symbols. Again, the integrated radar reflectivity is computed by column-integrating over reflectivity values (Z , not

dBZ), normalizing by the cloud depth, and then converting the integrated Z values into units of dBZ.

What is immediately obvious is the clear delineation between the optical depth of non-drizzling versus drizzling marine stratocumulus at optical depths of approximately 16. This result should not be interpreted as a physical means of categorizing drizzle from non-drizzle in a real cloud, as the boundary is purely an artificial product of the model autoconversion procedures. As is expected, the radar reflectivity/optical depth relationship is varied for the drizzle component, as the ‘clean’ run produced drizzle with much higher integrated reflectivity than did the ‘dirty’ case. By contrast, the non-drizzling and lightly-drizzling relationships are generally similar.

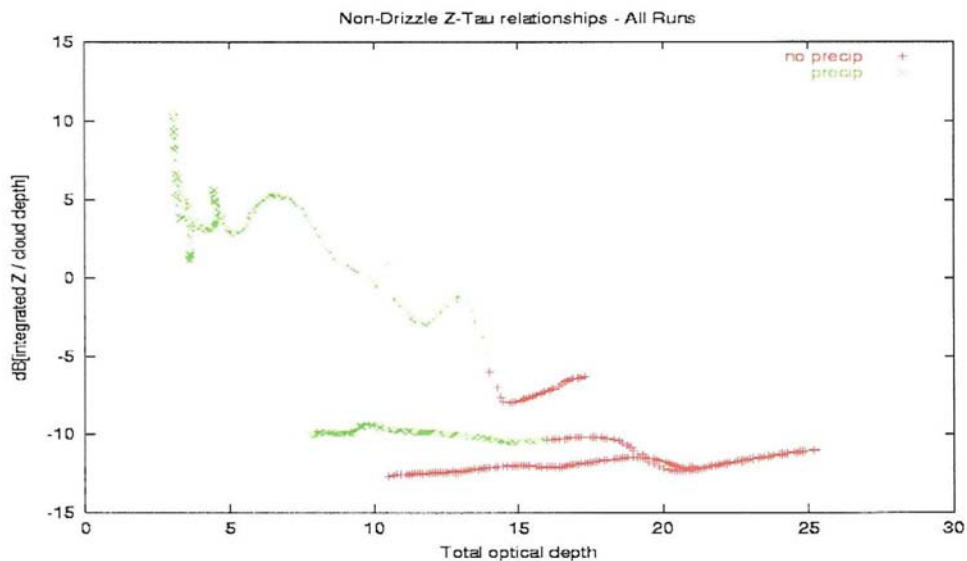


Figure 4.1. Montage of drizzle/non-drizzle radar reflectivity/optical depth relationships for all three runs of the CSU-CIMMS LES. Non-drizzle datapoints are represented by red symbols, while drizzle datapoints are represented by green symbols.

We note that the behavior of the drizzle signal is not easily predicted from the optical depth/radar reflectivity relationship, as the ‘dirty’ simulation radar reflectivity mirrors the relationship of the non-drizzle signal, while the ‘clean’ simulation drizzle signal departs significantly from the non-drizzle signature. This is, of course, a function of the radar reflectivity of the larger precipitation droplets, and illustrates the insensitivity of radar reflectivity to optical depth, as has been described in empirical studies of marine stratocumulus (e.g. Boers, 2002.)

4.2.a ‘Clean’ model run

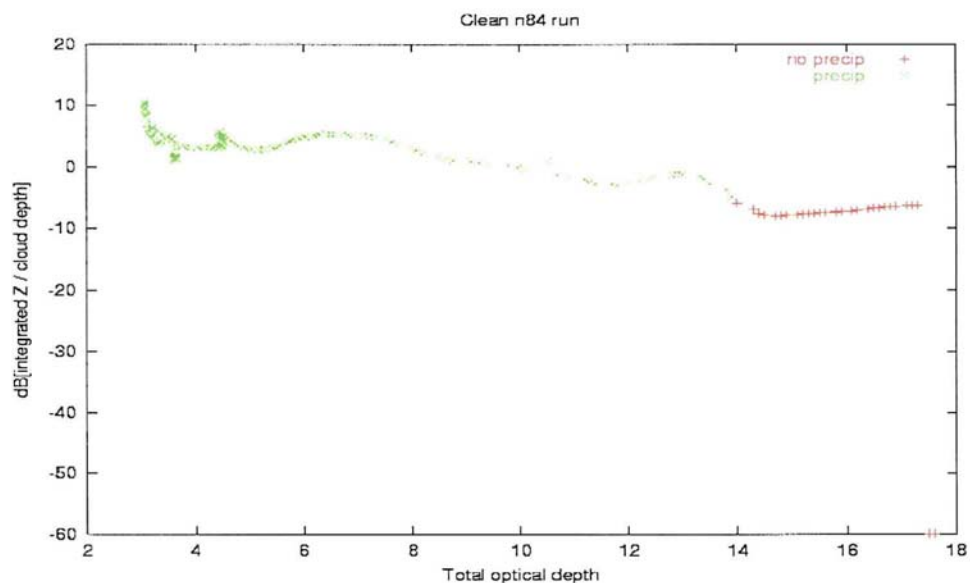


Figure 4.2. Radar reflectivity/optical depth measurement for the ‘clean’ run of the CSU-CIMMS LES model. Drizzle data is represented by green symbols, while non-drizzle data is represented by red symbols.

The reflectivity/optical depth relationship shown in Figure 4.2 indicates two distinct regimes: one for the period of drizzle when reflectivities are largely independent of optical depth, and a second regime of high optical depth and somewhat lower reflectivity representing non-drizzling cloud. Again, it is important

to note that the value of optical depth where the transition from one regime to the other is purely an artifact of the model's microphysics scheme (e.g., the point at which autoconversion of cloud water occurs) and as such, does not *depend* explicitly on the optical depth as simulated. Finally, the variable data found in the low optical depth regimes reflects the convective nature of the cloud near simulation's end.

This case contained rather heavy drizzle, and as such, is expected to differ somewhat from the two CAVEX cases described in Section 4.3, one of which contained no drizzle, the other, light drizzle. The 'clean' case, therefore, serves as a test of the retrieval under the duress of relatively strong drizzle. It is not expected that the retrieval should perform well, as strong drizzle negates the *a priori* assumptions made in the retrieval.

4.2.b 'Dirty' model run

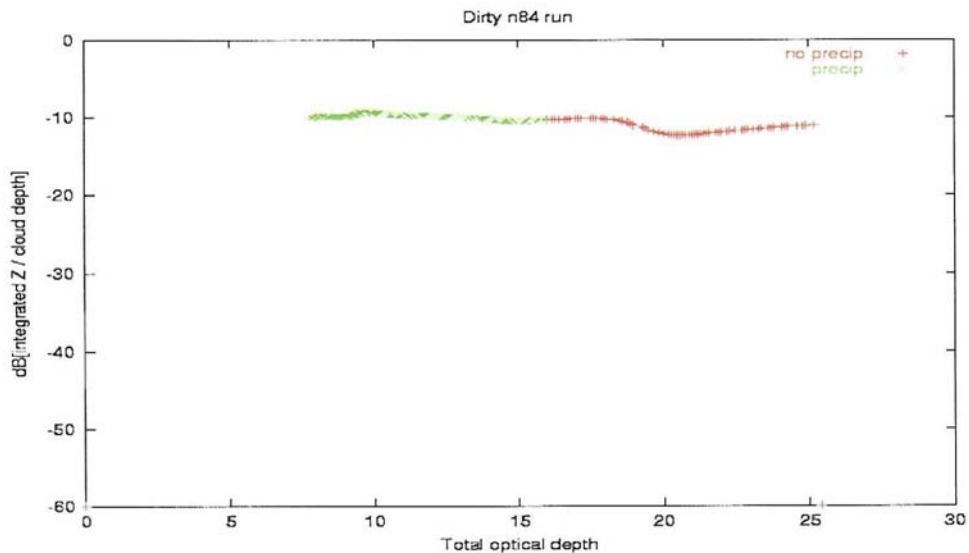


Figure 4.3. Radar reflectivity/optical depth measurement for the 'dirty' run of the CSU-CIMMS LES model. Drizzle data is represented by green symbols, non-drizzle by red.

Figure 4.3 presents the equivalent plot as in Figure 4.2, but for the ‘dirty’ simulation. The similitude of the drizzle and non-drizzle relationship to optical depth is of note. This is reflected in the general behavior of the total relationship as shown in Figure 4.3. Again, we see the clear delineation between drizzle and cloud at approximately $\tau = 16$ – still representative of the model’s microphysics, and not necessarily of any ‘real’ physics of the cloud layer. As would be expected, the similarity of the modelled drizzle radar reflectivity to the non-drizzle reflectivity should produce interesting results in the retrieval, as drizzle reflectivities and optical depths for this simulation are functionally similar to what one would expect for non-drizzling cloud at the same optical depths.

This case is fairly representative (in terms of total radar reflectivity and visible optical depth) of the CAVEX drizzle case of 24 July, 1999 (described in Part I of Austin and Stephens, 2000,) and should provide similar retrieval results as described in Part II of the same paper. One would expect the effect of drizzle to impede the retrieval accuracy, again due to the violations of the *a priori* assumptions caused by drizzle production. We will explore these results in Section 4.4.

4.2.c 'No Drizzle' model run

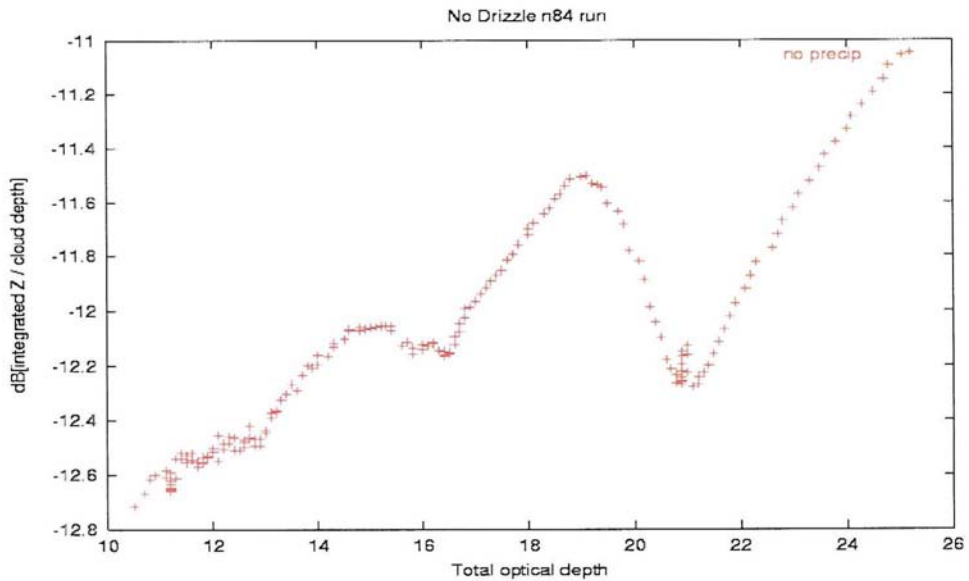


Figure 4.4. Radar reflectivity/optical depth measurement for the 'no drizzle' run of the CSU-CIMMS LES model. Non-drizzle data is represented by red symbols. No drizzle was produced by the simulation.

Figure 4.4 shows the radar reflectivity/optical depth relationship for the 'no drizzle' run. Note the difference in scale – the variability of the radar reflectivity/optical depth relationship for this simulation is less than 2 dBZ over the full range of optical depth, compared to perhaps 10 dBZ for the 'clean' simulation. For this purely hypothetical case, we see the extremely indifferent nature of the radar reflectivity/optical depth relationship for a non-drizzling cloud. Interestingly, the high-optical-depth part of this plot matches very nicely with the lower-optical-depth portion of the non-drizzling 'dirty' run, further suggesting the robustness of this non-drizzling case as a hypothetical 'super-aerosol content' cloud.

This simulation, as it fits the *a priori* assumptions the closest, should perform the best in the retrieval.

4.3 A Trial Retrieval Based on the Modelled Results

Having described the relevant parameters necessary for the retrieval process, we now apply the data presented above to the microphysical retrieval. The retrieval code described in Part I was obtained courtesy of Richard Austin, and was slightly modified by the author to accept the modelled input data files as opposed to the standard radar files. The code, titled the ‘CloudSat Antecedent Retrieval Algorithm 9’ is written in IDL, and serves as a prototype for the eventual operational CloudSat retrieval to be used (Dr. Richard Austin, personal communication.) The retrieval was applied to all three model runs, and the retrieved liquid water content and droplet effective radius were compared to the values produced by the model. The effects of drizzle become evident in the simulations which produced drizzle.

4.3.a ‘No Drizzle’ run

The idea behind the inclusion of this case was to evaluate the retrieval performance an ‘ideal’ model run with no drizzle. As such, we expect optimal agreement between the modelled parameters and the retrieved values based on the model input, especially considering the low error introduced into the retrieval by using simulated data. And indeed, we do see a 1:1 relationship between the retrieved values, and the simulated ‘truth.’ Figures 4.6 and 4.7 show time comparisons of modelled versus retrieved LWC and effective radius.

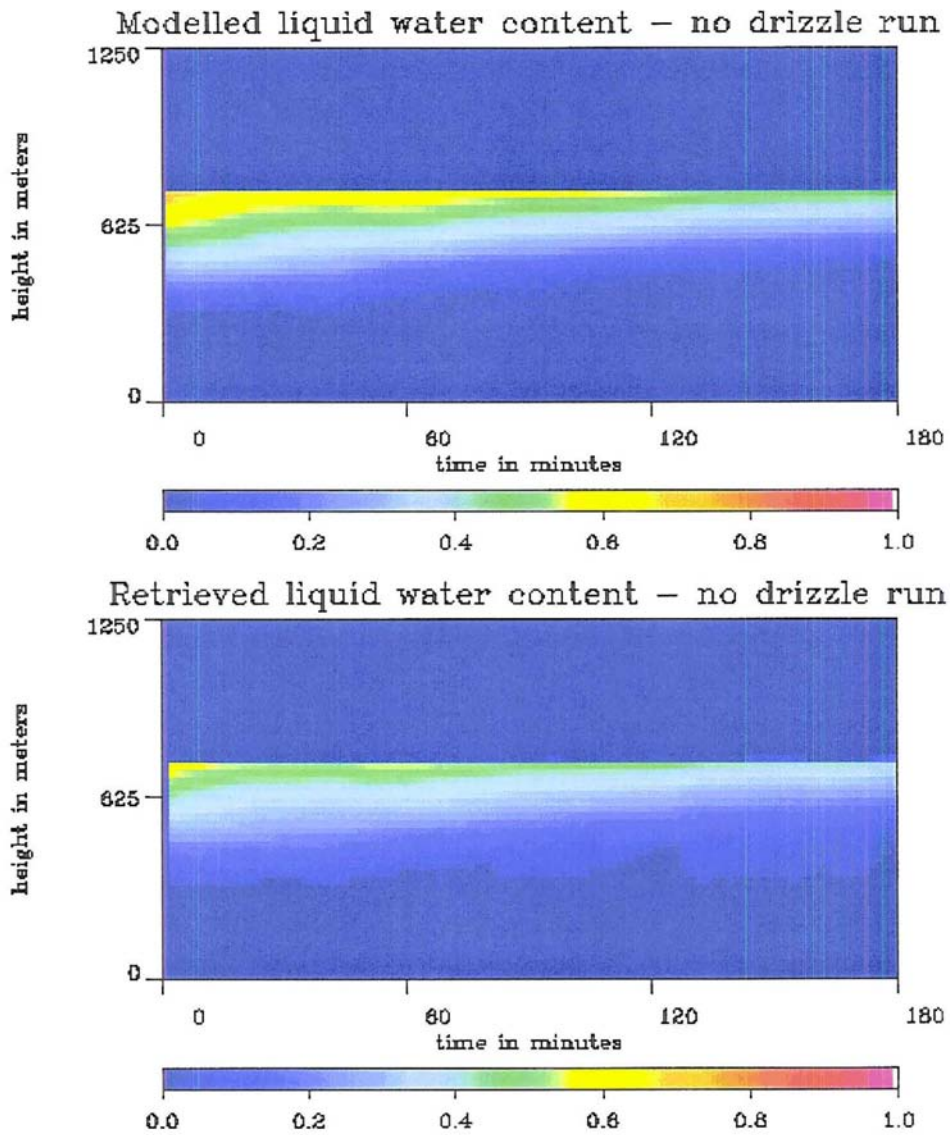


Figure 4.5. Time comparison of the modelled versus the retrieved liquid water content for the model. Values are horizontally averaged over the domain. Scale is in units of g/kg.

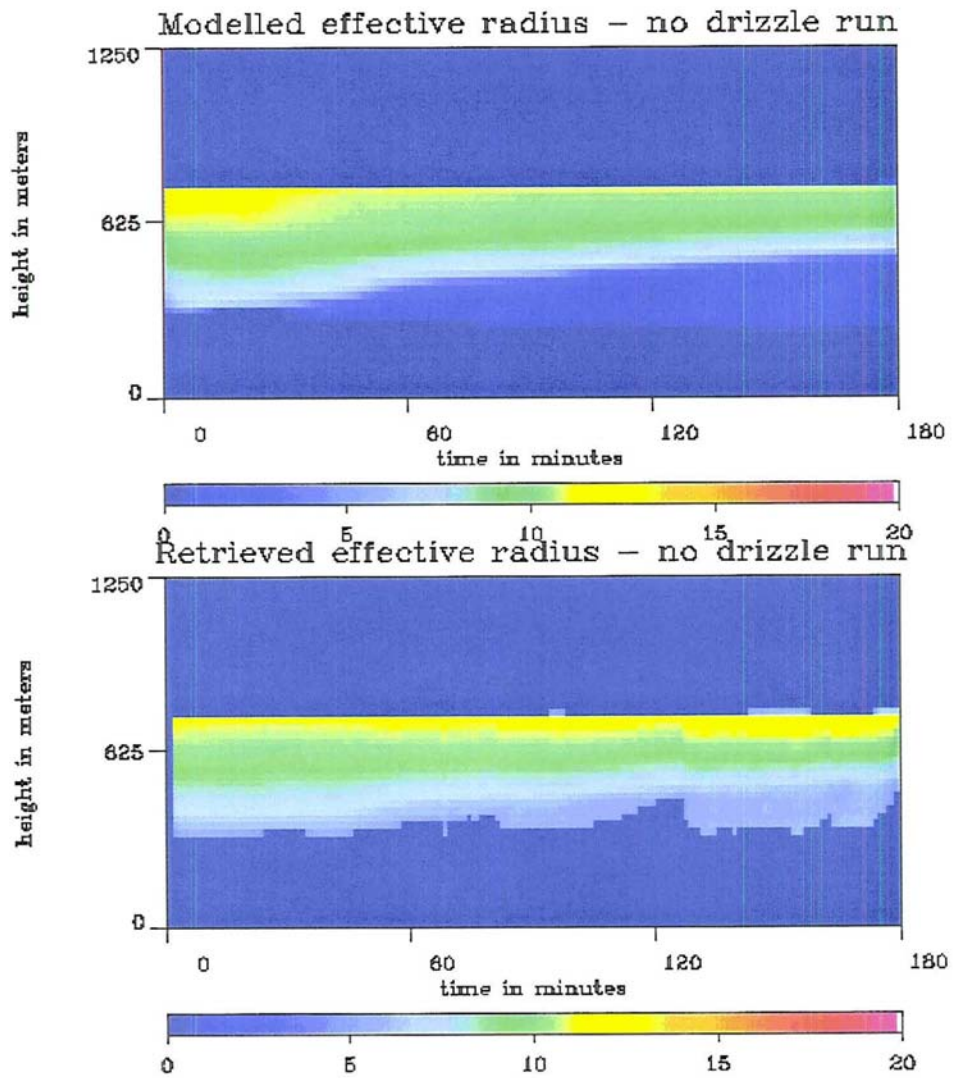


Figure 4.6. Time comparison of the modelled versus the retrieved effective radius for the model. Values are horizontally averaged over the domain. Scale is in units of microns.

As is seen in Figure 4.5, the retrieval does slightly underestimate the cloud-top liquid water content when compared to the modelled values. The liquid water content is, of course, a function of the cloud radius and the number concentration – as we see, the retrieval handles cloud radius parameters fairly well. The retrieval, however, makes the assumption that the number concentration of cloud droplets is constant as a function of height. Should this assumption not hold, or should the average value computed by the retrieval not match the values in the model, we would expect a deviance in the retrieved LWC as a result. We explore this discrepancy further in Section 4.5. Overall, the retrieval somewhat underestimates the total water path, likely as a result of this underestimation of number concentration. Figure 4.7 presents a comparison of modelled LWP to the retrieved values.

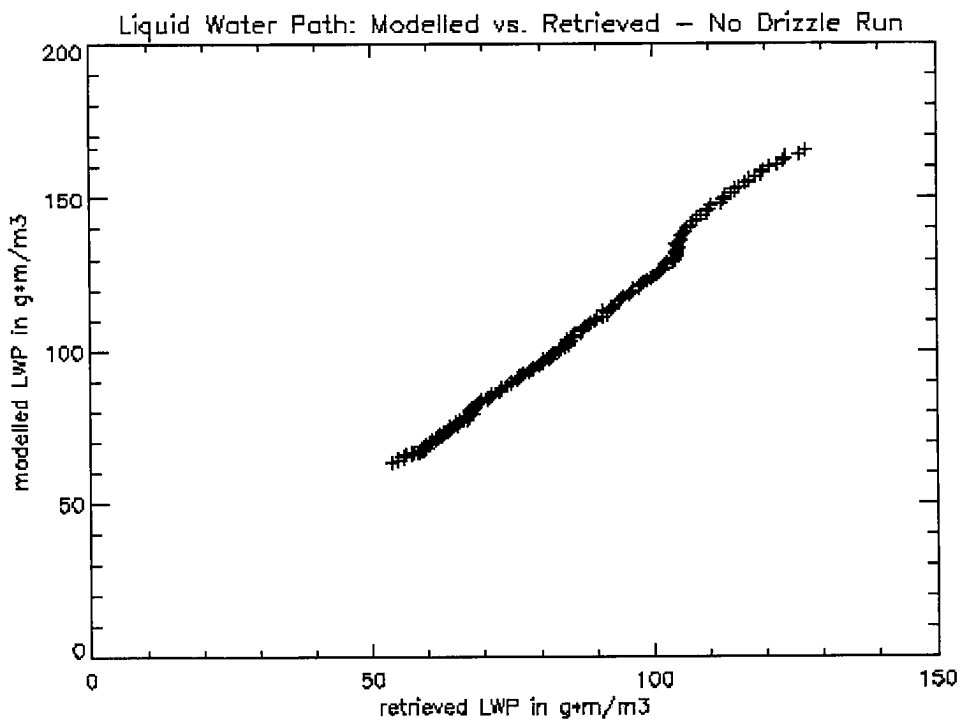


Figure 4.7. Comparison of LWP of the modelled and retrieved data for the 'no drizzle' simulation.

A direct comparison of the retrieved parameters to the modelled data is provided as Figure 4.8. The general agreement in the retrieved effective radius field is seen, as well as the slight underestimation of the LWC values.

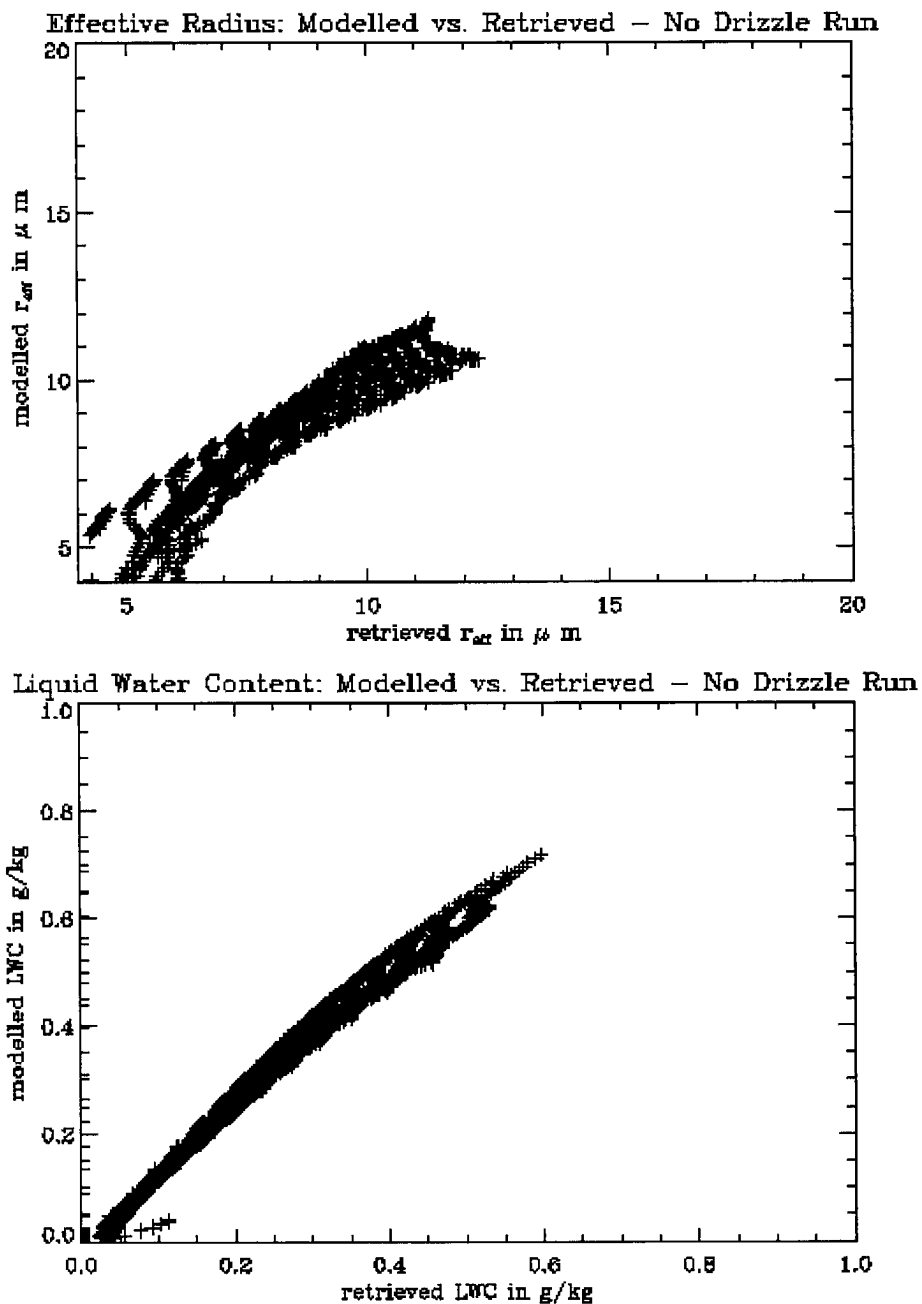


Figure 4.8. Comparison of the 'clean' case modelled data to the retrieved data.

4.3.b. 'Dirty' Case

The non-drizzling portion of the retrieval for this simulation performed similarly to the 'no drizzle' simulation: a slight underestimation of the retrieved LWC, due again to a cloud-top decrease in number concentration, but overall agreement. Of more interest is the fact that this is the first simulation containing drizzle to be analyzed by the retrieval. Figures 4.9 and 4.10 present the familiar comparisons between modelled and retrieved LWC and effective radius as a function of time.

As seen in Figure 4.9, the retrieval again slightly underestimates the liquid water content retrieval over the first 50 minutes or so of the simulation. Once drizzle begins to fall out of the cloud, the retrieval spreads the LWC out over the model, due to the influence of the stronger reflectivities lower in the cloud caused by the weak drizzle, and as such, the retrieval improves to near-total fidelity. The retrieval generally fares better for effective radius as seen in Figure 4.10. Especially interesting is the behavior of the retrieval once drizzle begins to fall from the cloud at approximately $t=70$ minutes. Drizzle droplets created by the model have radii of nearly $40\ \mu\text{m}$ – clearly violating the *a priori* assumptions made in the retrieval. However, the relative scarcity of these droplets results in only a mild overestimation of cloud effective radius on the order of $5\ \mu\text{m}$ or so near cloud bottom. We expect this overestimation to become larger, however, when the drizzle number concentration increases.

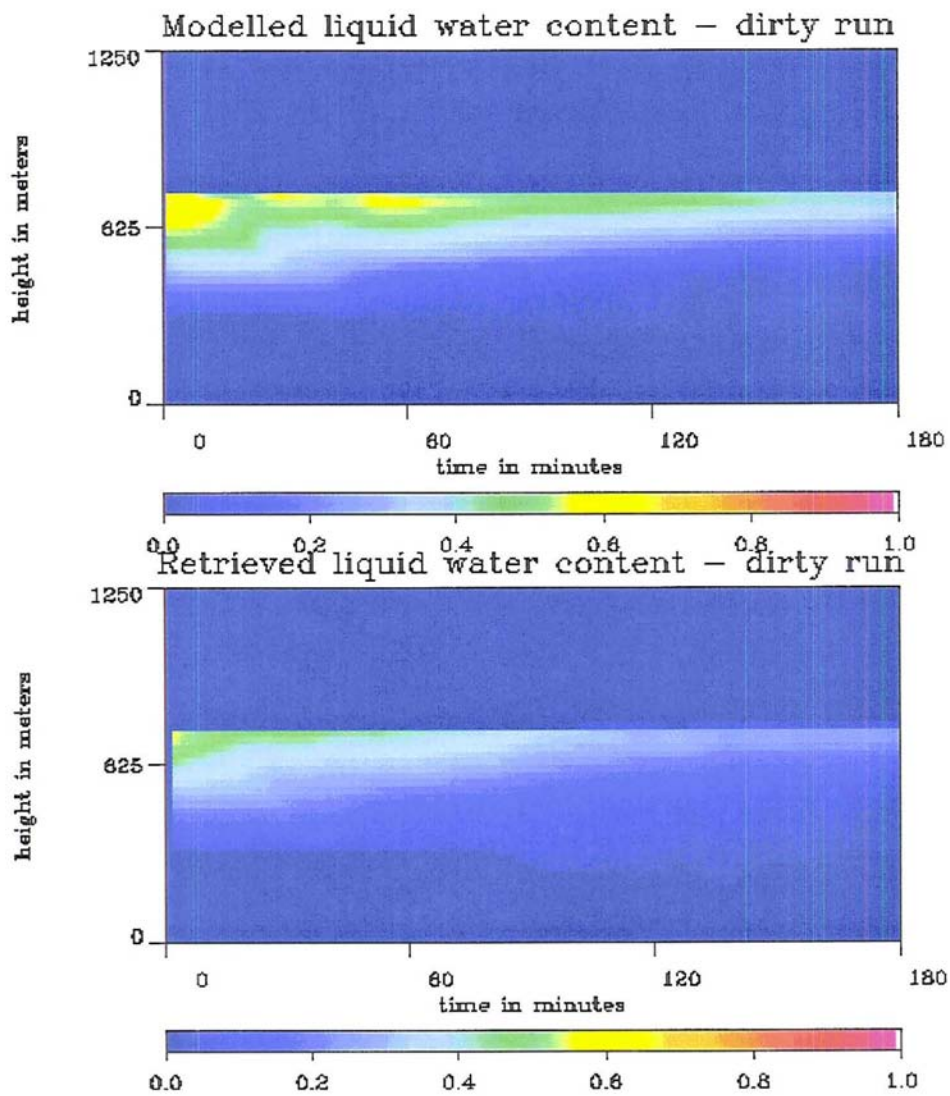


Figure 4.9. Time comparison of the modelled versus the retrieved liquid water content for the model. Values are horizontally averaged over the domain. Scale is in units of g/kg.

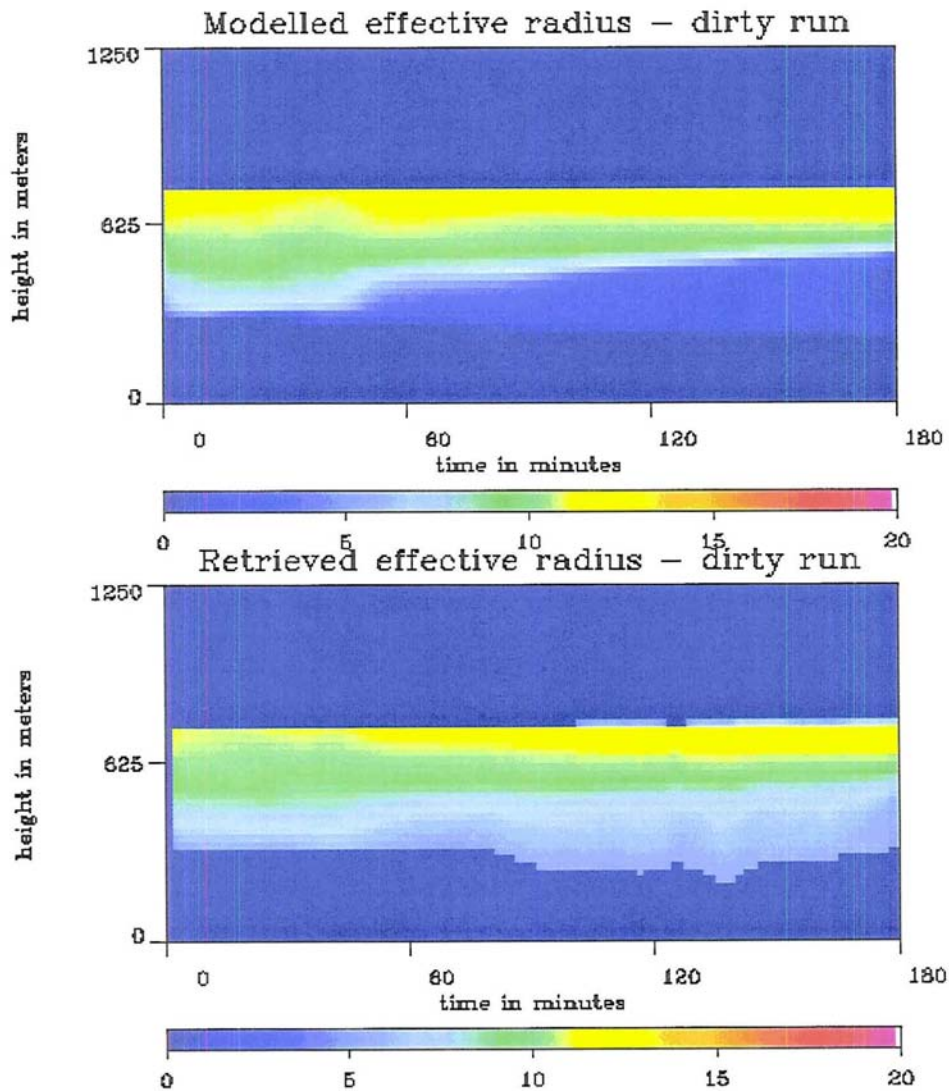


Figure 4.10. Time comparison of the modelled versus the retrieved effective radius for the model. Values are horizontally averaged over the domain. Scale is in units of microns.

As Figures 4.9 and 4.10 show, the effect of drizzle is very slight on this retrieval – the relative scarcity of drizzle hydrometeors when compared to the cloud is simply insufficient to completely dominate the radar reflectivity signature, and as such, produces only small changes in the retrieval. The retrieval underestimation of LWC is somewhat greater in this case, as is expected; drizzle hydrometeors are being formed through autoconversion of cloud liquid water, which leads to a distinct change in the vertical profile of cloud number concentration, especially at cloud top. Again, this violates the retrieval’s assumption that cloud droplet number concentration is constant with height, and produces a net underestimation of LWC near cloud top. As stated previously, we will explore this effect in more detail in section 4.4.

Figure 4.11 presents a comparison of the retrieved parameters versus the modelled data for the ‘dirty’ simulation, similar to Figure 4.8. We see the effect of drizzle formation first in the comparison of effective radii between the model and the retrieval; namely, the overestimation of effective radius by the retrieval of smaller droplets, found primarily in the lower section of the cloud during the drizzling portion of the simulation. Again, this is the region where large-radii drizzle droplets, albeit with low number concentrations, had an effect on the retrieval’s ability to retrieve droplet size. The underestimation of cloud LWC by the retrieval is seen as more pronounced than the ‘no drizzle’ simulation. Given that the deviations of cloud number concentration from the mean value are greater for this simulation when compared to the ‘no drizzle’ simulation; this is expected, as the assumption of constant number concentration is similarly less accurate for the ‘dirty’ simulation.

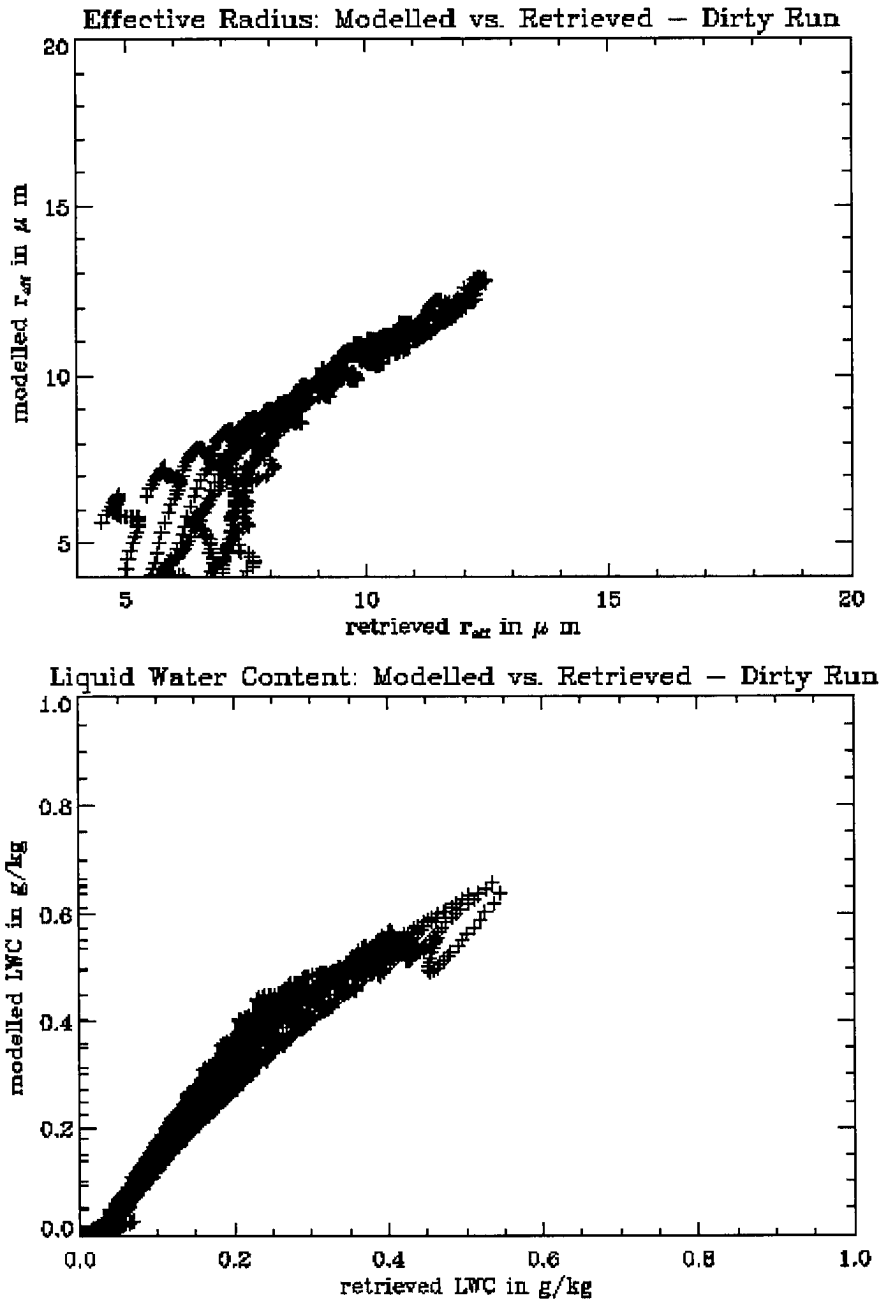


Figure 4.11. Comparison of the 'clean' case modelled data to the retrieved data.

4.4.c 'Clean' Model Run

As expected, the retrieval using data generated from the 'clean' simulation performed rather poorly. Of 180 available radar profiles, the retrieval succeeded in converging for only the first 51, essentially failing to retrieve any data whatsoever

from the last two hours of the simulation. This is not a total loss, however, as the reader will recall that the model produced significant drizzle in roughly the first 20 minutes of the simulation; as such, the retrieval did in fact sample some of the heavy drizzle produced by the model. The manner in which this heavy drizzle affects the retrieval will hopefully be instructive. Figures 4.12 and 4.13 present a comparison of modelled versus retrieved liquid water content, and effective radius, respectively.

As is seen in Figure 4.12, the retrieval underestimated liquid water content by roughly 50%. Given the radical variation of the cloud droplet number concentration from the mean value, this is not entirely unexpected. A further source of error in the retrieved LWC values is the gross underestimation of cloud droplet radii as seen in Figure 4.13. This underestimation of droplet radii would also lead to smaller retrieved values of LWC. Perhaps of more interest is the analysis of the retrieval of cloud droplet effective radii. Due to the relative scarcity of CCN in the simulation, cloud droplet growth was rapid enough to initiate autoconversion relatively early in the model simulation, leading to a decrease in optical depth. Until the drizzle began to fall from the cloud, the overall liquid water path remained constant – the combination of lower optical depth due to the presence of drizzle and a constant LWP led to a dramatic underestimation of cloud effective radius. As the simulation progressed, modelled effective radii continued to grow, and the retrieval of this parameter became progressively worse, until ultimately, the retrieval was unable to rectify the differences, and convergence became impossible.

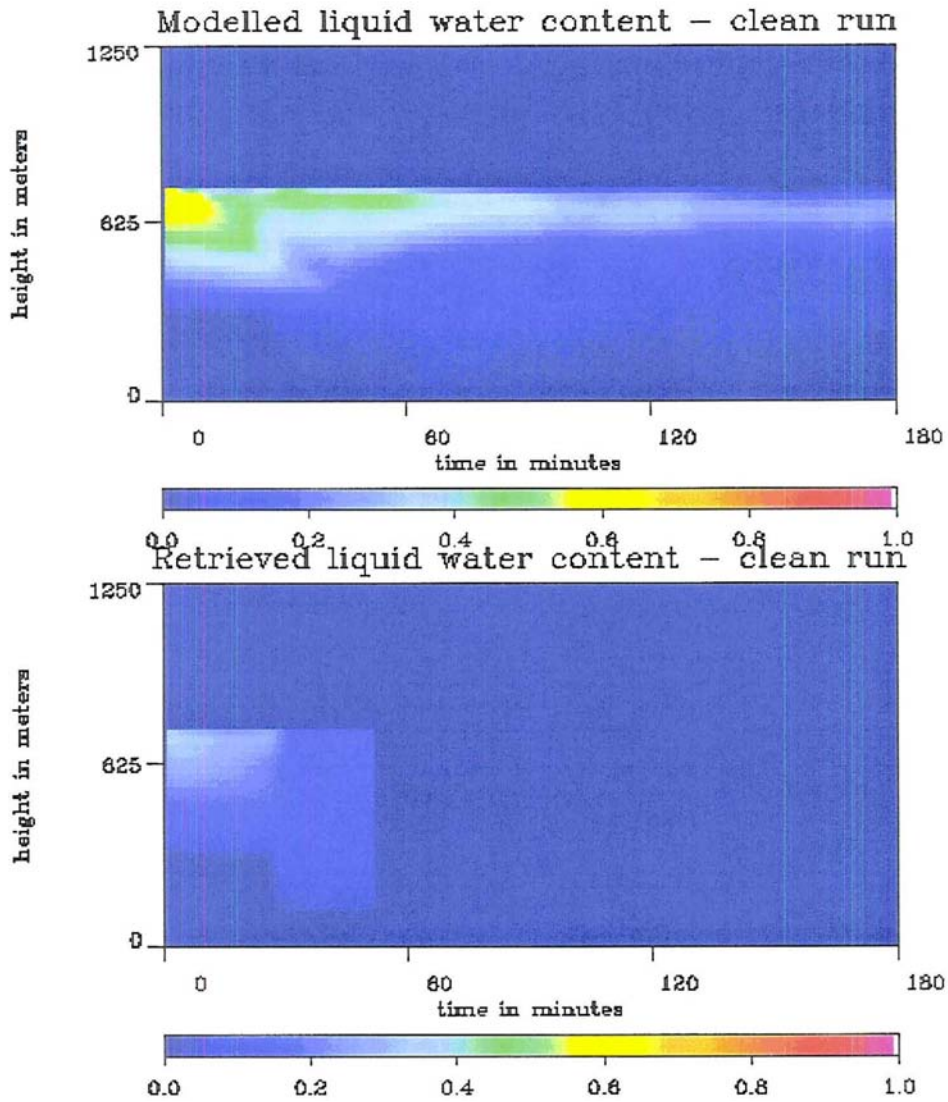


Figure 4.11. Time comparison of the modelled versus the retrieved liquid water content for the model. Values are horizontally averaged over the domain. Scale is in units of g/kg.

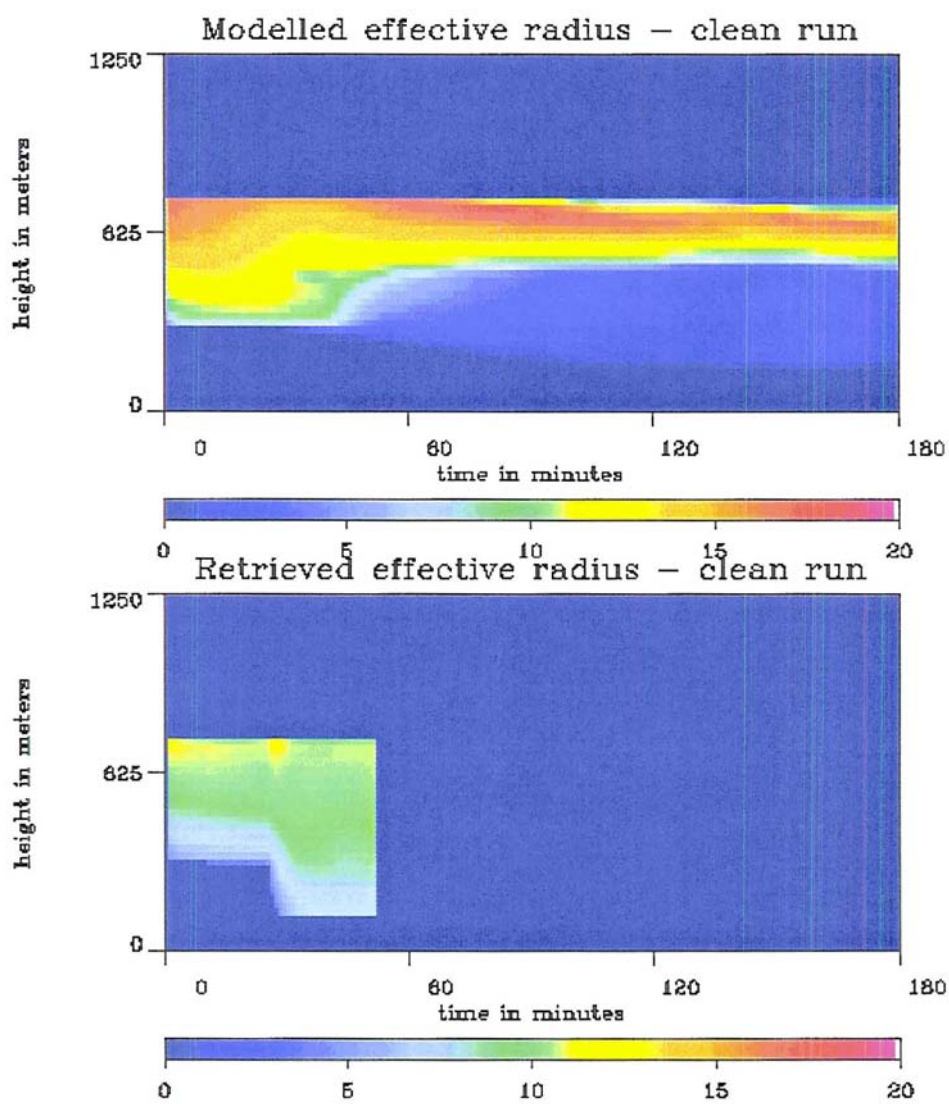


Figure 4.12. Time comparison of the modelled versus the retrieved droplet effective radius for the model. Scale is in units of microns.

Thus we the dominating role drizzle plays in this particular retrieval. For the ‘dirty’ simulation, the presence of drizzle did not dominate the radar reflectivity – for this simulation, the radar reflectivity signal was predominantly drizzle, and as such, the assumptions made in the retrieval simply did not fit the reality of the model. Figure 4.13 presents the familiar comparison of the retrieval versus the modelled data.

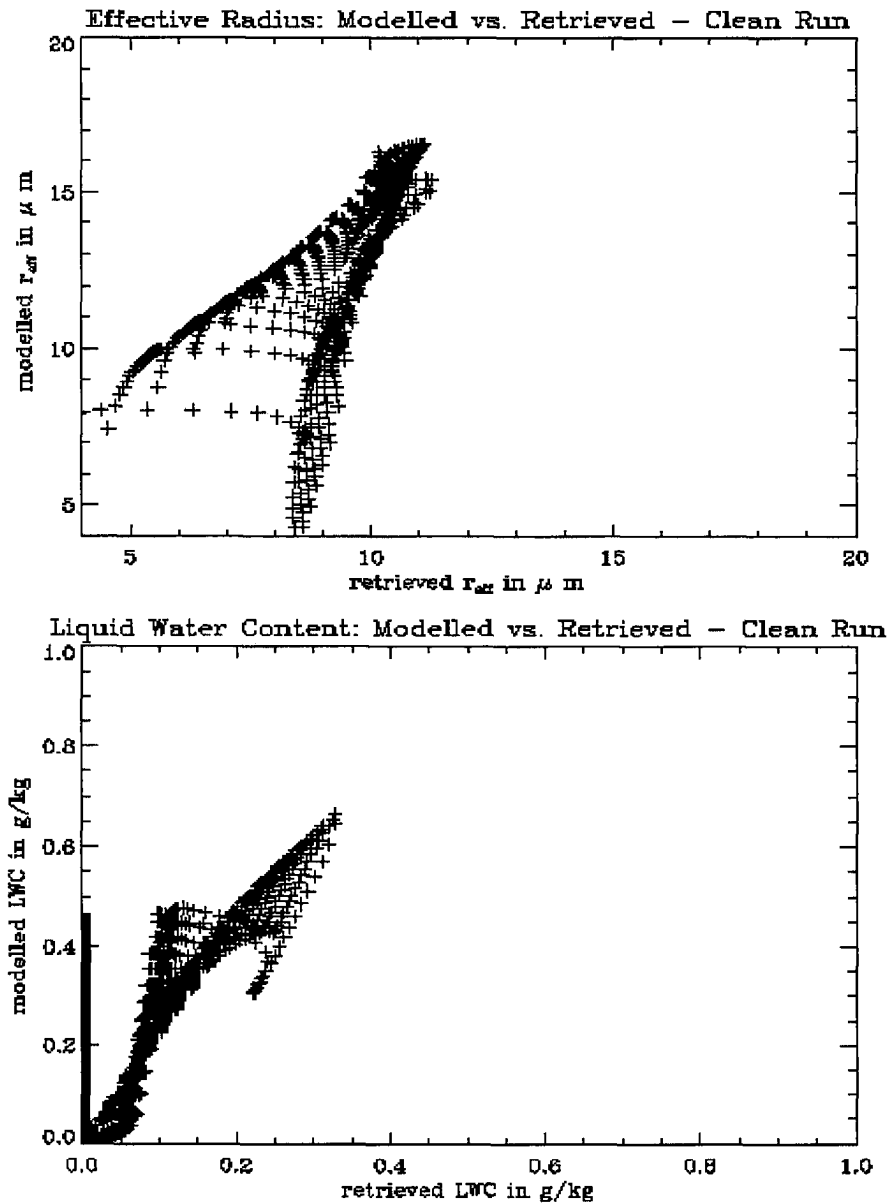


Figure 4.13. Comparison of the ‘clean’ case modelled data to the retrieved data.

The ‘clean’ simulation also produced the largest variances in cloud number concentration, coincident with the conversion of large amounts of cloud water to precipitation. This is, of course, another source of error in the retrieval. However, given the radical departures of the modelled radii values from the *a priori* assumptions, and especially considering the dominant role droplet radius plays in computation of radar reflectivity, we must assign the bulk of the error in the retrieval to the violation of the *a priori* assumptions.

4.4 Error Analysis

As described in Austin *et al.* (2002), the retrieval provides in the S_x matrix the variances of the retrieved properties r_g , N_T , as well as the variance of the size distribution parameter σ_{\log} . We calculate from these parameters the uncertainties (expressed, as in Austin *et al.*, in terms of the standard deviation) of the effective radius and liquid water content. These calculations follow through the standard formulae for propagation of errors, which are also described in Part II:

$$\begin{aligned} \delta r_{eff} &= \sqrt{\left(\frac{\partial r_e}{\partial r_g} \delta r_g\right)^2 + \left(\frac{\partial r_e}{\partial \sigma_{\log}} \delta \sigma_{\log}\right)^2}, \\ \delta LWC &= \sqrt{\left(\frac{\partial LWC}{\partial N_T} \delta N_T\right)^2 + \left(\frac{\partial LWC}{\partial r_g} \delta r_g\right)^2 + \left(\frac{\partial LWC}{\partial \sigma_{\log}} \delta \sigma_{\log}\right)^2} \end{aligned} \quad (4.6)$$

Given the definitions for the liquid water content and effective radius as described in equations (6) and (7) in Austin and Stephens (2002), we can trivially compute the differential terms in equation 4.6 and use the uncertainties calculated by the retrieval

to compute the overall uncertainty (again, expressed in terms of the standard deviation) for the desired output parameters.

We compute the overall uncertainties for effective radius and liquid water content for the lightly-drizzling ‘dirty’ simulation, as well as for the ‘no-drizzle’ simulation. We neglect the heavy drizzling ‘clean’ simulation, as the retrieval fails to converge on physical values after approximately $t=51$ minutes. This leads to extremely unpredictable behavior in the retrieval output parameters for this simulation, especially in the number concentration field, which at the end of the failed retrieval, is reported by the retrieval to be negative. This naturally cannot be, and so we postulate that there is no benefit to performing an analysis of error on results that are manifestly non-physical. The other simulations, upon which the retrievals converge *in toto*, are of more interest, as the retrieved results are not only physical, but consistent with observed results.

The ‘no-drizzle’ simulation provided the optimum situation for the retrieval mechanics, and not surprisingly, the best error estimates. The retrieval reported fractional uncertainties in r_g , N_T , and σ_{\log} of roughly 8%, 11%, and 23%, respectively: from these values we calculate the fractional uncertainty for the effective radius to be $\sim 13\%$, and for the liquid water content to be $\sim 31\%$. The results are as expected: the uncertainty in the LWC is higher than that of the effective radius as the computation of the LWC is a function of r_g , N_T , and σ_{\log} , while the effective radius depends only on r_g , and σ_{\log} . These results are slightly smaller (on the order of a few percent) than retrieval uncertainties reported by Austin *et al.* for a non-drizzling retrieval of California marine stratocumulus; this is not surprising, as the highly regulated ‘no-

drizzle' simulation is likely a better fit for the retrieval than a real cloud, as the real cloud would have more stochastic variance than does the numerically 'perfect' simulated cloud.

For the lightly-drizzling 'dirty' simulation, the variances in number concentration, as well as the larger spread of droplet radii, leads to slightly larger errors. Interestingly enough, the computed fractional uncertainties for r_g , N_T , and σ_{\log} are smaller than in the 'no-drizzle' case with values of ~7%, 9%, and 23%, respectively. This is not surprising, as the optical depths for the 'dirty' simulation were lower than for the non-drizzling simulation, and since the error estimate for optical depth is represented in the retrieval code as a percentage of the optical depth, we are left with numerically smaller values of the retrieved parameters, after carrying out the propagation of error. The computed total uncertainties, of course, are higher, due to the larger effect of the change in the differential terms of equation 4.6. For the 'dirty' simulation, we compute uncertainties of effective radius and liquid water content to be ~16% and ~62%, respectively. These, not surprisingly, are larger than for the 'no drizzle' simulation, and are more in line with reported results by Austin *et al.* (2002). Furthermore, we see the effect of drizzle on the uncertainties: by creating a larger spread in droplet radii, as well as a change in number concentration, we increase the numerical value of the computed differential terms in equation 4.6 and as such, increase the overall uncertainty of the parameter.

In the Part II paper by Austin *et al.* (2002), it is shown that the computed uncertainties are consistent with observed uncertainties as seen through *in situ* measurements: as we have no *in situ* uncertainties present in our modeled data, we

cannot duplicate this comparison. However, given that the error analysis methodology is identical to that described in the Austin *et al.* (2002) we believe the error analysis presented here to be reliable information, and report the estimates as such.

4.5 Effects of Drizzle on the Radar Reflectivity/Optical Depth Retrieval

The ordering of the three retrievals presented above is intended to describe a progressive analysis of the effects of stronger and stronger drizzle on the retrieval process. As drizzle begins to form in the simulations, it affects the radar reflectivity and visible optical depth in the manner described in Chapter 3. Since the retrieval is designed for the paradigm of cloud-only retrievals, the variances introduced by the presence of drizzle result in progressively worse violations of the *a priori* assumptions made in the retrieval. As we have seen, the retrieval consistently underestimates cloud liquid water content and effective radius in the presence of drizzle, even the extremely light drizzle manifested in the ‘dirty’ simulation. As the algorithm is simply not equipped to constrain a retrieval containing drizzle droplets whose radii are an order of magnitude larger than the *a priori* assumptions, we cannot expect any other results. Perhaps a useful addition to the retrieval would be an independent analysis of cloud liquid water path – obtained through passive microwave instruments, for example – which would provide another constraint in the retrieval algorithm.

Of course, the retrieval knows nothing of the changes in the microphysical constitution of the marine stratocumulus system brought about by the onset of drizzle– it ‘sees’ only radar reflectivity and optical depth, and must proceed basing its

results on the assumptions made. For the ‘no drizzle’ simulation, the assumptions made in the retrieval are perfectly valid, and the retrieval performs well. The ‘clean’ simulation presents a roughly similar picture in terms of radar reflectivity, and only somewhat lower optical depths than the ‘no drizzle’ simulation – however, the microphysical structure which constitutes the radar reflectivity and optical depth for the ‘clean’ case is vastly different than the ‘no drizzle’ simulation – violating the assumptions made in the retrieval – and as such, the retrieval performs poorly. The key lesson here is that the information contained in the observational parameters is, of course, more important than the parameters themselves. We have seen how two different clouds can produce similar observational parameters. Of great benefit, perhaps, would be the inclusion of an additional parameter, such as an independently retrieved LWP estimate, in the assimilation of this data to further constrain the information produced from the observations. As we saw in Chapter 3, for a constant LWP, a drizzling cloud will have a markedly lower optical depth and higher radar reflectivity than a non-drizzling cloud containing the same LWP. This kind of analysis would no doubt improve retrieval of cloud microphysical parameters by allowing for better identification and pre-processing of realtime data.

Another consistent feature of the retrieval we see is a consistent underestimation of cloud liquid water, especially at cloud-top. Generally, cloud top is where one would expect to find the largest cloud droplets; given the functional relationship between cloud droplet size and the autoconversion process, we would expect the simulated cloud-top to be a region where a large amount of autoconversion of cloud water to drizzle – resulting in a decrease of cloud number concentration, in violation

of the assumptions made in the retrieval. As such, a possible hypothesis for the biasing of cloud liquid water content at cloud top would be this variation in cloud droplet number concentration at cloud top. This hypothesis is easy to test due to the complete knowledge of the cloud microphysics as produced by the model: we can trivially compare profiles of cloud droplet number concentration produced in the model simulations with the average value computed by the retrieval.

Figure 4.14 presents a profile of horizontally- and time-averaged cloud number concentration for all three model simulations as compared to the mean cloud number concentration computed by the retrieval. The ‘no drizzle’ simulation is represented by solid lines, the ‘dirty’ simulation is represented by dotted lines, and the ‘clean’ simulation by dashed lines.

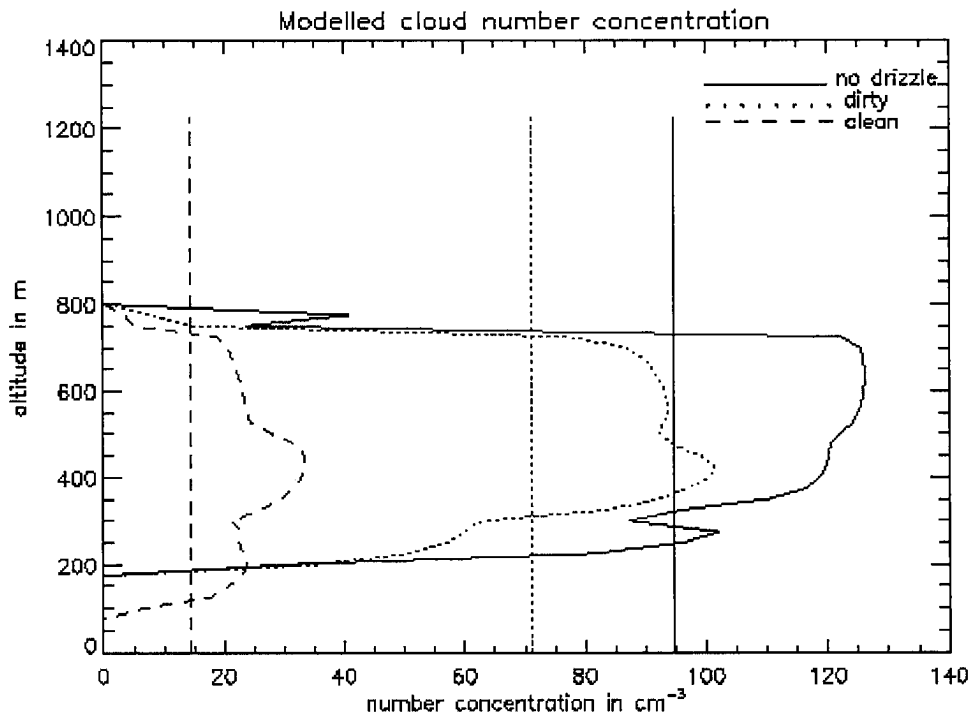


Figure 4.14. Profile of horizontally- and time-averaged cloud and drizzle number concentrations for all three model simulations. Vertical lines correspond to the mean, constant values computed by the retrieval for each case.

As seen in Figure 4.14, the retrieval generally underestimates the cloud number concentration by around 15%. Furthermore, we can see the effect of drizzle in the simulated data represented above. Each simulation appears to consist of three regimes – a cloud bottom layer from ~200-350 m, a cloud mid-layer, from ~350-500m, and a cloud-top layer from ~500-700 m. All three cloud-bottom layers show reasonable decreases in cloud number concentration – the dropoff is sharp and would constitute a well-defined cloud bottom. The mid-layers of the simulations represent the domain of predominantly cloud droplets of average size, while the upper cloud layers would represent the largest cloud droplets. In the drizzling cases, however, we see a marked decrease in this top layer, due to the autoconversion of these larger cloud droplets to drizzle. Further reinforcing this hypothesis is the slight *increase* in cloud number concentration for the lone non-drizzling simulation in this cloud-top region. What we observe, therefore, are general underestimations by the retrieval on the order of 15% for all simulations, and for the drizzling simulations, an additional decrease in cloud number concentration at cloud top, worsening the underestimation of the retrieval. Given the direct relationship between liquid water content and cloud number concentration, these underestimations of cloud number concentration would suggest an underestimation of liquid water content in the retrieval of equal magnitude. As is seen in Figure 4.8, the general underestimation is on the order of perhaps 0.03 g/kg or a deviation of approximately 15%. This supports the hypothesis that errors in the computation of number concentration result in the biases produced by the retrieval. And as expected, these biases become slightly worse in the drizzling simulations, as again would be expected by the increase in deviation from the mean

number concentration produced by the model. We therefore conclude that the most likely source of the slight bias in the retrieved LWC fields are due to the errors of the number concentration calculation performed in the retrieval.

Overall, we have seen the general utility of the retrieval for non-drizzling and lightly-drizzling marine stratocumulus. We also show how the retrieval can fail under heavy drizzle; fortunately, we have found in Chapter 3 that it is possible to discriminate these heavy drizzling cases based on the observations themselves. What remains is to construct a method whereby retrieval of these drizzling cases becomes quantitative; this is left as research yet to be performed.

Chapter Five

Conclusions and Future Work

5.1 Summary

We have presented research combining LES modelling with remote retrieval of cloud microphysical parameters using radar reflectivity and visible optical depth. The cloud systems simulated were based on observed marine stratocumulus as described by Nicholls (1984) and were constructed to explore the effect of aerosol concentration on precipitation formation. The simulated results agreed well with observations made with the Nicholls study. After computing radar reflectivity and optical depth based on the modelled output, we compute a theoretical relationship between the two parameters, and show this relationship holds in the simulated radar reflectivity and optical depth. Furthermore, the simulated results match with observations – both in the theoretical relationship of radar reflectivity and cloud optical depth, as well as with physical observations of cloud and drizzle radar reflectivity components. Specifically, we show evidence supporting the partitioning of cloud and radar reflectivity as shown in Baedi, Boers, and Russchenberg (2001) and expand upon this empirical finding by examining the upper limit suggested by the theoretical analysis of the optical-depth/radar reflectivity relationship. Based this analysis combined with model results, we are able to construct a qualitative identification process allowing for discrimination of drizzling marine stratocumulus from non-drizzling systems.

We then apply the simulated reflectivity and optical depth data to a cloud microphysical retrieval, and show that for non-drizzling and lightly-drizzling marine stratocumulus systems, the retrieval performs well. We explore the manner in which

the retrieval fails for heavy-drizzling systems, based on assumptions made in the retrieval and on the effects precipitation in the cloud system has on the assumptions made.

5.2 Conclusions

The utility of satellite-based remote sensing systems such as the CloudSat platform will no doubt enhance our understanding of the global environment, and as such, enriches our understanding of the natural universe. For example, current space-based radar systems (such as the TRMM mission) are simply incapable of detecting the kind of light precipitation that CloudSat system has the capable of analyzing. The ability to quantify the rainrates of these lightly-precipitating systems will further our understanding of the global energy budget, as there exists little statistical data about the latent heat fluxes associated with these systems. Further analyses of the interactions between clouds and the earth-atmosphere system are nearly limitless given the quantity and quality of observations that will soon exist, and we must endeavor to make full use of these opportunities. Through the modelling and subsequent analysis of cloud systems we soon hope to observe directly, we can prepare more thoroughly for the future, and make full use of the opportunities afforded us by systems such as the CloudSat instrument.

5.3 Future Work - On the Quantification of Drizzle Properties Based On Observations

The results presented over the last four chapters suggest the inclusion of a third cloud microphysical parameter to assist in the identification of drizzle. Should this become a reality, the natural progression would be to apply a

drizzle retrieval for observed data that is flagged as drizzling, thus quantifying the drizzle component and increasing the overall value of the retrieval. Cloud liquid water path is perhaps a valuable parameter to consider – it may be retrieved using passive microwave sensors (thus satisfying the requirement that additional data be independent of the other measurements, namely radar reflectivity and visible optical depth) and as has been shown above, allows for more confidence in the identification of drizzling marine stratocumulus.

We propose to explore this possibility by utilizing a precipitation-rate retrieval by L'Ecuyer and Stephens (2002) combined with independent LWP data to serve as the means of quantifying drizzle information. As such, the model used for this simulation will, in the coming months, be used to simulate a broad variety of drizzling and raining systems, and the retrieval of L'Ecuyer will be analyzed and optimized to perform the necessary retrievals. Combined with the results of the CloudSat Antecedent cloud retrieval, the resulting retrieval system should provide the means to a wealth of information about the marine stratocumulus system not currently available to researchers.

References

- Ackerman, A.S., O.B. Toon, and P.V. Hobbs, 1995: A model for particle microphysics, turbulent mixing, and radiative transfer in the stratocumulus-topped boundary layer and comparison with measurements. *J. Atmos. Sci.*, **52**, 1204-1236
- Austin, R.T., and G.L. Stephens, 2000: Retrievals of stratus microphysical parameters using millimeter-wave and visible optical depth in preparation for CloudSat: Part I: Algorithm formulation. Submitted, *Journal of Geophysical Research*
- , -----, S.D. Miller, S.M. Sekelsky, F. Li, and Q. Min, 2000: Retrievals of stratus microphysical parameters using millimeter-wave and visible optical depth in preparation for CloudSat: Part II: Algorithm evaluation. Submitted, *Journal of Geophysical Research*
- Baedi, R., R. Boers, and H. Russchenberg, 2001: Detection of boundary layer water clouds by spaceborne cloud radar. Pre-press.
- Blake, D., 1928: Temperature inversions at San Diego, as deduced from aerographical observations by airplane. *Monthly Weather Review*, **56**, 221-224.
- Charlson, R.J., J.E. Lovelock, M.O. Andreae, and S.G. Warren, 1987: Ocean phytoplankton, atmospheric sulfur, cloud albedo, and climate. *Nature*, **326**, 655-661.
- Clark, T.L., 1974a: A study of cloud phase parametrization using the gamma distribution. *J. Atmos. Sci.*, **31**, 142-155.
- Deardorff, J.W., 1972: Numerical investigation of neutral and unstable planetary boundary layers. *J. Atmos. Sci.*, **29**, 91-115.
- , 1980: Cloud-top entrainment instability. *J. Atmos. Sci.*, **37**, 131-147
- Fritsch, A.S., C.W. Fairall, and J.B. Snider, 1995a: Measurement of stratus cloud and drizzle parameters in ASTEX with a K_a -band doppler radar and a microwave radiometer. *J. Atmos. Sci.*, **52**, 2788-2799.
- Gierasch, P. and R. Goody, 1970: Models of the Venus clouds. *J. Atmos. Sci.*, **27**, 224-245.
- Herman, G. and R. Goody, 1976: Formation and persistence of summertime arctic stratus clouds. *J. Atmos. Sci.*, **33**, 1537-1553

- Kessler, E., 1969: On the distribution and continuity of water substance in Atmospheric circulations. *Meteor. Monogr.*, **No. 32**, Amer. Meteor. Soc., 84 pp.
- Khairoutdinov, M., 1998: Large-eddy simulation of stratocumulus-topped boundary layer with an explicit and a new bulk microphysics scheme. Cooperative Institute for Mesoscale Meteorological Studies Report no. 108, University of Oklahoma, Norman, OK, 144 pp. [Available from the Cooperative Institute for Mesoscale Meteorological Studies, Norman OK 73019]
- , and Y. Kogan, 2000: A new cloud physics parametrization in a Large-Eddy Simulation model of marine stratocumulus. *Mon. Wea. Rev.*, **128**, 229-243
- L'Ecuyer, T.S. and G.L. Stephens: An Estimation-Based Precipitation Retrieval Algorithm for Attenuating Radars. *J. Appl. Meteor.*, **41**, 272-285
- Lilly, D.K., 1968: Models of cloud-topped mixed layers under a strong inversion. *Quart. J. Roy. Meteor. Soc.*, **94**, 294-309
- Lorenz, E.N., 1963: Deterministic nonperiodic flow. *J. Atmos. Sci.*, **20**, 130-141.
- Marshall, J.S., and W. McK. Palmer, 1948: The distribution of raindrops with size. *J. Meteor.*, **5**, 165-166
- Mason, P.J., 1994: Large Eddy Simulations: A critical review of the technique. *Quart. J. Roy. Meteor. Soc.*, **120**, 1-26
- Miller, S.D., G.L. Stephens, C.K. Drummond, A.K. Heidinger, and P.T. Partain, 2000: A multisensor diagnostic satellite cloud property retrieval scheme. *J. Geophys. Res.*, **105**, 19 955-19 971
- Moeng, C.-H., 1986: Large-eddy simulation of a stratus-topped boundary layer. *J. Atmos. Sci.*, **43**, 2886-2900
- Nicholls, S., 1984: The dynamics of stratocumulus: Aircraft observations and comparisons with a mixed layer model. *Quart. J. Roy. Meteor. Soc.*, **110**, 783-820
- Ramanathan, V., R.D. Cess, E.F. Harrison, P. Minnis, B.R. Barkstorm, E. Ahmad, and D. Hartman, 1989: Cloud-radiative forcing and climate: Results from the earth radiation budget experiment. *Science*, **243**, 57-63
- Randall, D.A., 1980: Conditional instability of the first kind upside-down. *J. Atmos. Sci.*, **37**, 125-130.

- , J.A. Coakley, Jr., C.W. Fairall, R.A. Kropfli, and D.H. Lenschow, 1984: Outlook for research on subtropical marine stratiform clouds. *Bull. Amer. Met. Soc.*, **65**, 1290-1301.
- Rodgers, C.D., 1976: Retrieval of atmospheric temperature and composition from remote measurements of thermal radiation. *Reviews of Geophysics and Space Sciences*, **14**, 609-624.
- Sadowy, G.A., et al., 1997: The NASA DC-8 airborne cloud radar: Design and preliminary results. *Proc. IGARSS 1997*, **4**, 1466-1469.
- Salby, M.L., 1996: *Fundamentals of Atmospheric Physics*. Academic Press, 627pp.
- Sassen, K. et al., 2002: Unknown Title. *In Preparation*.
- Sommeria, G., 1976: Three-dimensional simulation of turbulent process in an undisturbed trade wind boundary layer. *J. Atmos. Sci.*, **108**, 407-426.
- Stephens, G.L., R.F. McCoy Jr., R.B. McCoy, P. Gabriel, P.T. Partain, and S.D. Miller, 2000: A multipurpose scanning spectral polarimeter (SSP): Instrument description and sample results. *J. Atmos. and Ocean. Tech.*, **17**, 616-627.
- Stephens, G.L., S.-C. Tsay, P.W. Stackhouse Jr., and P.J. Flatau, 1989: The relevance of the microphysical and radiative properties of cirrus clouds to climate and climatic feedback. *J. Atmos. Sci.*, **47**, 1742-1753.
- Stephens, G.L., 1994: *Remote Sensing of the Lower Atmosphere*. Oxford University Press, 523pp.
- Stevens, B., 1996: On the dynamics of precipitating stratocumulus. Department of Atmospheric Science Paper 618, Colorado State University, Fort Collins, CO, 140pp. [Available from the Department of Atmospheric Science, Colorado State University, Fort Collins, CO 80523.]
- Stull, R.B., 1999: *An Introduction to Boundary Layer Meteorology*. Kluwer Academic publishers, 670pp.
- Warren, S.G., C.J. Hahn, J. London, R.M. Chervin, and R.L Jenner, 1988: Global distribution of total cloud cover and cloud type amounts over the ocean. U.S. Department of Energy Rep. DOE, ER-0406 212pp.
- Young, K.C., 1993: *Microphysical Processes in Clouds*. Oxford University Press, 427pp.

Appendix A: Mie versus Rayleigh Radar Reflectivities

These values were computed by Tristan L'Ecuyer and Angela Benedetti, and the values included below were taken from the numbers provided by Drs. L'Ecuyer and Benedetti.

Freq(GHz)	Wavelength(um)			
94.000	3191.5			
P. Rate(mm/hr)	R_eff(um)	Chi_e	LWC(g/m^3)	
0.0350	180.951	0.3562	0.002661	
Temp.(K)	Ref. Index (r,i)			
300.0	3.527970	2.191673		
sig_Ext.	sig_Sca.	sig_Abs.		
6.529584E-08	1.804462E-08	4.725144E-08		
K^2	Z(cm3)	eta_Ray(cm-1)	eta_Mie(cm-1)	
0.814	1.070727E-12	2.570463E-08	2.362828E-08	

Computing the ratio of eta_Ray to eta_Mie yields ~1.08, or an overestimation of ~8% of the Rayleigh approximation compared to Mie theory.